Silver Nanowire-enhanced Microflake Electrically Conductive Adhesives for Flexible Hybrid Electronics

by

Hubert Argasinski

A thesis
presented to the University of Waterloo
in fulfillment of the
thesis requirement for the degree of
Master of Applied Science
in
Electrical and Computer Engineering (Nanotechnology)

Waterloo, Ontario, Canada, 2021

Author's Declaration

I hereby declare that I am the sole author of this thesis. This is a true copy of the thesis, including any required final revisions, as accepted by my examiners.

I understand that my thesis may be made electronically available to the public.

Abstract

Flexible hybrid electronics combine the power and performance of conventional integrated circuits with the large area, lower cost, and mechanical flexibility of printed, flexible electronics. To mount rigid, discrete components on printed, flexible circuits, a conductive, flexible, and mechanically binding interconnect is required. The high processing temperature of solder, the gold standard for conventional electronics, is not compatible with mechanically flexible substrates such as plastics, textiles, and paper. Furthermore, solder is brittle and lead-based solders are slowly being phased out due to new environmental regulations. Electrically conductive adhesives (ECAs) are one of the most promising alternatives to solder for flexible hybrid electronics since their low processing temperatures are compatible with flexible substrates. However, ECAs are brittle and their resistance greatly increases upon repeated strain, which is not ideal for bendable devices. And although they exhibit excellent conductivity, it is still not as high as solder.

Silver microflakes are the most commonly used conductive filler in ECAs, however, the flakes lose contact with each other under mechanical strain. In this work, silver nanowires are added to microflake ECAs as an auxiliary filler to improve the flexibility and conductivity of the ECA. The silver nanowires bridge neighbouring microflakes improving the conductivity, and the long reach and flexibility of the nanowires can maintain an electrical connection under strain. The fabrication procedure, as well as the concentration and dimensions of the nanowires, are studied and optimized for flexible ECAs.

Ultrasonication is one of the most popular mixing methods for ECAs but it is found in this work that the nanowire-containing ECA is sensitive to the duration. During the initial phases, up to 10 min., the sonication works to disperse the conductive fillers in the epoxy resin, which is beneficial, while beyond 10 min. the sonication damages the nanowires, degrading their performance. The next parameter of interest was the nanowire to microflake ratio for a fixed silver content. If too little nanowires are added, the ECA underperforms, and if too many nanowires are added, they agglomerate on the surface of the microflakes. It was found that the optimal nanowire to microflake ratio for long and thin nanowires was 1:5, and 1:4 for short and thick ones. Lastly, it was found that the longest and thickest nanowires show the most improvement in the electrical and mechanical properties of the ECAs as their larger diameter makes them more resilient to damage and their long reach helps keeps the network in contact when stretched.

By narrowing in on the steps and parameters relevant to nanowires, resistivities as low as 3.9 x 10^{-4} Ω·cm are achieved, compared to 1.9 x 10^{-3} Ω·cm for the baseline flake-only ECA. After 100 cycles to 30% strain, the resistance of the hybrid nanowire/microflake ECA increased only 9.8x, compared to 25x for the flake-only ECA. The hybrid ECA demonstrated a higher maximum elongation of 120% compared to 75% for the flake-only ECA. Meanwhile, a commercial ECA broke while being strained to 30%. Shorter and thicker nanowires showed better shear strengths than longer and thinner nanowires, but the shear strength of all the hybrid ECAs was lower than the flake-only ECAs. However, it is demonstrated the strength is still sufficient in a real-world device by integrating a light emitting diode on a flexible substrate using the ECA. The device using the pure flake ECA broke after 256 cycles to 20% strain, while the device using the hybrid ECA showed no change in intensity after 500 cycles.

Acknowledgements

I would like to thank God for the many blessings in my life and for providing me with the opportunities that allowed me to get to where I am now. I would like to thank the Blessed Mother without whose strength and intercession, I would not have been able to complete this work.

I would like to thank my parents, Janusz and Maria Argasinski, for their love and support throughout my degree. Whether it was a hot meal on the weekend or calling to check-in, they were there for me. I would also like to thank my brother, Przemysław, his wife, Sylwia, and their son, Oliver, for their love, support, and encouragement. I would also like to thank all of my friends and family for their continued support.

I am thankful to my labmates, Muhammed Kayaharman, Jonathan Atkinson, Tianqi Li and Tiancheng Xu, for all of our valuable discussions inside and outside of the lab.

I would like to sincerely thank Professor Irene Goldthorpe for her guidance throughout my project. I am grateful for her external patience and continued support during the different obstacles encountered over the course of this work, especially during the unprecedented COVID-19 pandemic. I would also like to thank Dr. Marwa Abd-Ellah for her guidance while Professor Goldthorpe was away.

Finally, I would like to acknowledge the help of the Fatigue and Stress Analysis Lab, in particular Dr. Behzad Behravesh, for allowing me access to their equipment and running the single-lap shear strength tests.

Table of Contents

List of Figures

List of Tables

List of Abbreviations

AgMf	Silver microflake
AgNP	Silver nanoparticle
AgNW	Silver nanowire
API	Application programming interface
BADGE	Bisphenol A diglycidyl ether
CAGR	Compound annual growth rate
CNT	Carbon nanotube
DGEBA	See BADGE
ECA	Electrically conductive adhesive
E-textile	Electronic textile
FHE	Flexible hybrid electronic
IC	Integrated circuit
LED	Light-emitting diode
Mf	Microflake
NW	Nanowire
PCB	Printed circuit board
PEN	Polyethylene naphthalate
PET	Polyethylene terephthalate
PVP	Poly(vinyl pyrrolidone)
SEM	Scanning electron microscopy
SL	Short length
TETA	Triethylenetetramine
TPU	Thermoplastic polyurethane

UL	Ultralong
VISA	Virtual instrument software architecture
wt%	Weight percent

Chapter 1
Introduction

1.1 Printed Flexible Electronics

1.1.1 Overview

Printed, flexible electronics are revolutionizing the way we interact with technology allowing devices to conform to and move with the surface they are mounted on. From foldable phones to wearable health monitoring devices and rollable solar cells, they are opening new, diverse applications for electronics. Compared to conventional printed circuit boards (PCBs), which use a subtractive manufacturing process where the conductive traces are etched from a copper plated board, printed, flexible electronics are manufactured through an additive process, i.e., printing. Different printing methods, such as aerosol jet, inkjet, and screen printing, are used to deposit functional inks on paper, textiles, and plastics such as polyethylene terephthalate (PET), polyethylene naphthalate (PEN), and thermoplastic polyurethane (TPU). Compared to conventional electronics, printed, flexible electronics offer numerous advantages including a lower cost, larger areas, higher fabrication throughput, decreased prototype turnaround time and a conformable form factor.

The global flexible electronics market is expected to reach $25 billion USD by 2026 with an compound annual growth rate (CAGR) of 18% [1]. One of the fastest growing sectors of the printed, flexible electronics market is smart textiles, also known as electronic textiles or e-textiles, which is expected to reach $5.55 billion USD by 2025 with a CAGR of 30% [2]. The growth is driven by increased interest in wearable technology and a growing number of applications, especially in healthcare. Growth in the related smartphone market has accelerated smart textile market growth by enabling numerous applications such as personal health monitoring.

1.1.2 Printed Flexible Hybrid Electronics

While printed, flexible electronics offer many advantages, their performance cannot compete with certain conventional electronic devices such as silicon integrated circuits (ICs). Printed flexible hybrid electronics (FHEs) integrate the flexibility, low cost and large areas of printed, flexible electronics with the high performance and low power consumption of conventional (opto)electronics devices such as microcontrollers, analog-to-digital convertors, and light-emitting diode (LEDs) [3]. A typical composition of an FHE setup is shown schematically in Figure 1-1a). Conductive traces, usually made

from silver ink, are printed on a flexible substrate, and discrete, rigid components such as microchips are mounted over top. An encapsulating layer protects the printed circuit from environmental factors, such as humidity and physical abrasion. Because the mounted devices are small in comparison to the entire circuit, the larger hybrid device can still bend and stretch as most of the strain is incurred by the substrate and printed, flexible conductive traces. In some cases, the FHEs can be further designed to keep the rigid components away from joints and other mechanically active areas.

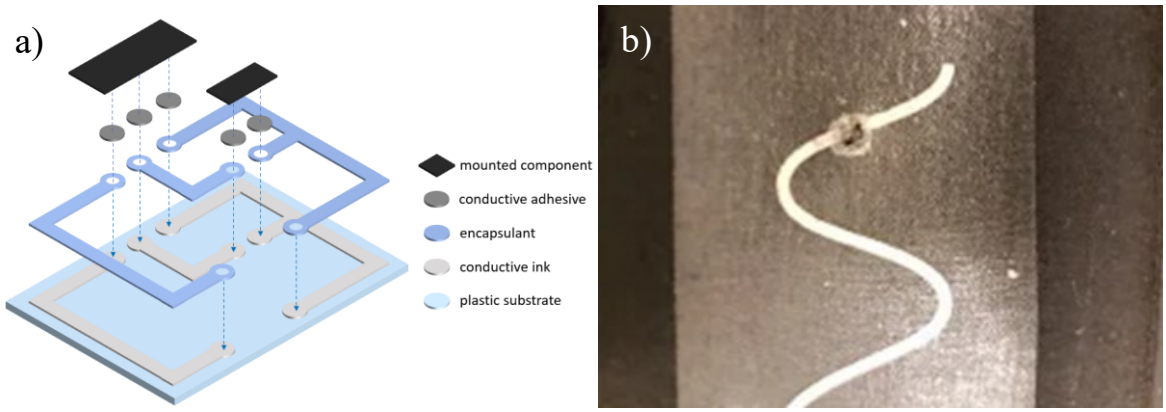

Figure 1-1: a) Typical composition of flexible hybrid electronics. It consists of printed traces on a flexible substrate, with rigid device components mounted on top. b) A printed, flexible circuit trace damaged by the high temperature required to deposit solder.

The rigid components require an electrical and mechanical connection to the printed conductive traces. Solder is the gold standard for mounting components onto a conventional PCB, but it has a high processing temperature: 204 °C for tin-lead (Sn-Pb) solder [3]. This temperature is too high for the vast majority of flexible substrates. An attempt at depositing solder on an in-house circuit trace printed on TPU and laminated onto a fabric is shown in Figure 1-1b), demonstrating that both the conductive line and the substrate are damaged. Furthermore, solder is brittle and thus cracks upon bending and stretching, compromising, and sometimes severing both the adhesive and electrical connection. It also does not adhere properly to plastic substrates, and new environmental regulations are limiting the use of lead-based solders [4].

1.1.3 E-textiles

E-textiles are FHEs integrated onto textiles. Devices can be integrated into clothing, furniture, bedding, vehicle interiors among many other possibilities, and the devices range from sensors [5]–[8] and displays [9]–[11] to nanogenerators [12]–[14] and photovoltaics [15]–[17]. As we are in contact with textiles the vast majority of the day, the seamless integration of devices onto those textiles is of growing

interest for applications in the internet of things, health and home care, fitness tracking, defense, automotive, construction, food packaging and fashion. For instance, pressure sensors integrated directly into the sheets of a bed could help immobile patients from developing bed sores [18].

One approach to e-textile fabrication is to weave conductive yarn into fabric, however the differing mechanical properties of conductive yarn (increased stiffness, brittleness, etc.) compared to regular yarn makes it difficult to work with and unpleasant for the end user. The more prevalent method used by industry is to instead apply the techniques of printed flexible electronics to deposit electronics on the surface of fabric. This allows the separation of the technology layer from the textile layer, which allows the device integration to occur outside of the textile manufacturing facility. Typically, FHEs are printed on a thermoplastic polyurethane (TPU) substrate, which is then heat laminated onto a textile.

Currently, one of the main limitations of e-textiles, as with the broader area of FHEs, is the lack of a conductive, flexible, mechanically-binding interconnect. Electrical connections, with mechanical strength and flexibility, are required between the printed conductive traces and microcontrollers, batteries, etc. Similar to conventional electronics, access to a conductive interconnect would enable modularity in e-textiles and FHEs – different components could be printed separately, potentially using incompatible processes, and then brought together at the end during an assembly step. As aforementioned, solder has been applied with limited success due to it is high processing temperature, brittleness, and poor adhesion to flexible substrates. An ideal e-textile interconnect would be conductive, flexible, durable, and printable. Various options have been explored to fulfill these requirements with some of the earliest being mechanical methods, such embroidery, i.e. sewing on components using a conductive thread [19], crimping [20] and poppers (snaps) [21], [22]. Despite the excellent strength of the connection, embroidery suffers from the limitations of conductive threads: they are stiff, difficult to work with and add extra steps to fabrication. Likewise, crimping and poppers offer excellent mechanical strength, but are rigid and require modification of the components being mounted. For instance, one end of the snap must be attached to the component being mounted on the e-textile.

1.2 Electronically Conductive Adhesives

1.2.1 Background

Electrically conductive adhesives, or ECAs, are one of the most promising technologies for conductive, flexible mechanical connections that would help overcome the limitations of the techniques described

thus far (i.e. solder, textile snaps, etc.). They have a low processing temperature, adhere to a wide range of substrates, require fewer processing steps and can be mechanically flexible. An ECA is a material that mechanically bonds two other materials and creates an electrical pathway between them. It consists of a polymer matrix, which defines the mechanical properties, and a conductive filler, which defines the electrical properties. Additional additives may be added to modify the final properties of the ECA. There is a tradeoff between the mechanical and electrical properties – as more conductive filler is added to improve the electrical properties, the mechanical properties degrade. The composition of a typical ECA is shown in Figure 1-2.

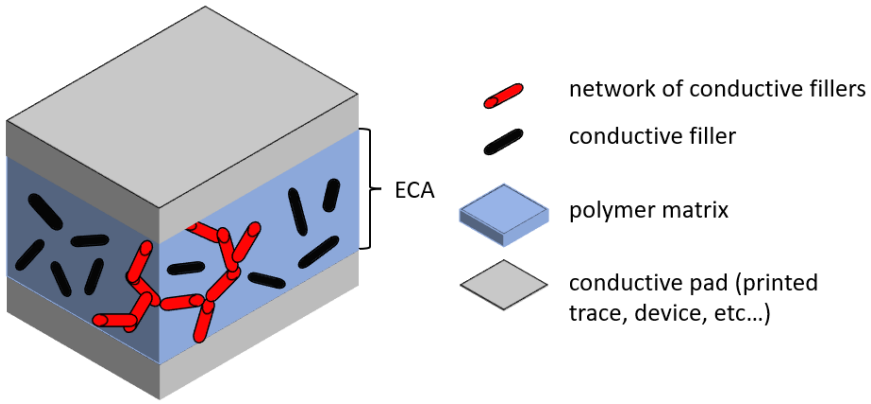

Figure 1-2: The typical composition of an electrically conductive adhesive (ECA).

Commercially, ECAs are available worldwide from several companies including DuPont, Henkel, MG Chemicals, Atom Adhesives and Master Bond, among others. In industry, they are predominantly used for lead frame die attachment and backplane attachment in solar cells. Commercially available ECAs are predominantly epoxy-based and use silver microflakes (AgMfs) as their conductive filler. Silver is used as it is the most conductive metal and relatively stable in air compared to other metals. The main limitations preventing the widespread use of ECAs in printed, flexible electronics include poor mechanical properties [23]–[25] and lower-than-desired conductivity [23] and adhesion strength.

1.2.2 Polymer Matrix

The choice of the material for the polymer matrix depends on the desired mechanical properties of the composite, with epoxy resins [26]–[28], polyurethanes [28], [29] and silicones [30], [31] being popular choices. Broadly, the polymer matrix can be classified as thermoplastic or thermoset depending on whether the curing reaction is reversible or not, respectively. Thermoplastics are cured through cooling and due to the reversibility of the curing, thermoplastic based ECAs are reworkable, like solder [32].

This means that if a component is damaged, or a connection was not established, the circuit can be easily repaired by reheating, i.e. softening, the ECA. On the other hand, thermosets are cured through a reaction with a curing agent, often referred to as a hardener. With the help of catalysts, thermosets may even be cured at room temperature. During curing, a three-dimensional cross-linked structure is created, which results in shrinkage of the matrix. This applies a compressive force on the conductive filler reducing the resistance of thermoset based ECAs [33], [34]. Thermosets also offer better heat and chemical resistance and adhesion strength than thermoplastics.

One of the most common choices for an epoxy-based ECA is the epoxy resin bisphenol A diglycidyl ether, also known as D.E.R.™ 332, BADGE or DGEBA [28], [35]–[37]. It is a thermosetting resin cured with triethylenetetramine, TETA. DGEBA-based epoxies exhibit many favorable properties for the polymer matrix of an ECA including high moisture resistance, good heat and chemical resistance, low viscosity, and good mechanical properties [38]. Good moisture, chemical and heat resistance is especially important for ECAs aimed at e-textiles as the garment will be exposed to sweat from the user and laundry detergent and abrasive forces during washing.

1.2.3 Conductive Filler

The other main component of an ECA is the conductive filler which creates the electrical connection between the components joined by it. Ideally, the conductive filler would have a high conductivity to facilitate the transfer of electrons and be able to maintain that conductivity with repeated bending/stretching. The size, shape and nature of the material all influence its conductivity and viability as a conductive filler. Further, the conductive filler should not hinder the mechanical properties of the polymer matrix by requiring a high fill fraction.

1.2.3.1 Conductivity Mechanisms

The conductive pathway through the insulating matrix is created through percolation - a conductive network formed by conductive fillers in contact - and tunneling mechanisms [27]. Percolation theory states that a conductive pathway through an insulating material will be achieved once the amount of randomly distributed filler surpasses a critical value, called the percolation threshold. The percolation threshold depends on the size, shape, and agglomeration of the filler. Higher aspect ratio structures, such as nanorods, nanotubes and nanowires, will have a lower percolation threshold than lower aspect ratio structures, such as microflakes and nanoparticles [39], as demonstrated in Figure 1-3. This means that less conductive filler is required to achieve conductivity. Below the percolation threshold, there

may be localized conductive networks, but the conductivity of the composite will be low or negligible. There may be some conductivity as electrons may hop between neighbouring conductive fillers through tunneling. If the electron has enough energy, it may overcome the potential barrier, and hop from one conductive filler to the next, even if the fillers are not in contact. The likelihood of an electron tunneling between fillers depends on the distance between them. Even if two fillers are in contact, the electron may have to tunnel through thin, insulating films present on the surface of the fillers. Once the fill fraction of the conductive filler reaches the percolation threshold, the conductivity rapidly increases as there is a continuous conducting pathway throughout the composite. A typical conductivity profile for a composite around the percolation threshold is shown in Figure 1-4. When the conductive filler reaches the percolation threshold, the conductivity of the composite increases by approximately twelve orders of magnitude. Adding more filler beyond this point has less of an impact on the conductivity and primarily serves to increase the robustness of the system.

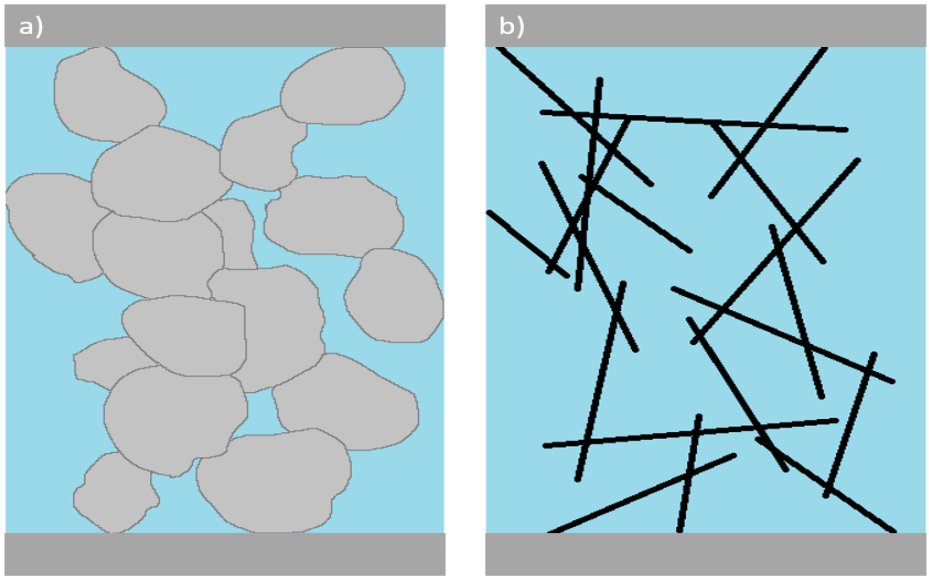

Figure 1-3: The percolation threshold dependence on the aspect ratio of the conductive filler. a) Silver microflakes have a low aspect ratio and require a high fill fraction to create a continuous conductive network through the matrix. b) Higher aspect ratio structures require a lower fill fraction.

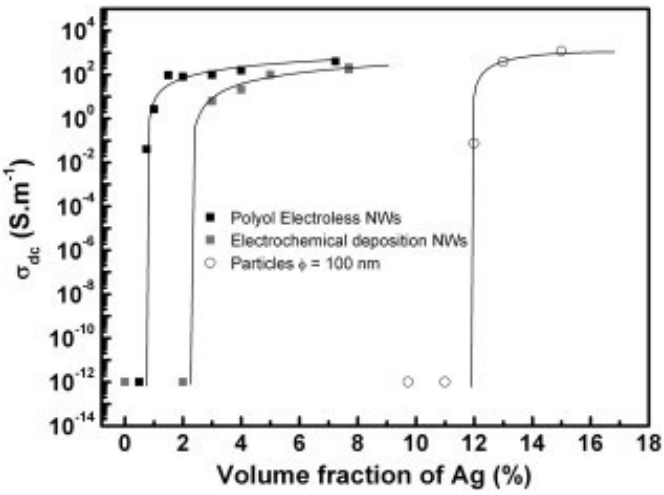

Figure 1-4: The percolation threshold of three different silver nanofillers in a P(VDF-TrFE) matrix, from [40] **(NWs = nanowires). (Reprinted with permission from Elsevier).**

From the conductivity mechanisms, the resistance of an ECA can be defined as:

$$R_{ECA} = R_f + R_{f\text{-}f} \tag{1}$$

where R_{ECA} is the overall resistance of the ECA, R_f, also referred to as R_b, is the bulk resistance of the conductive filler and $R_{f\text{-}f}$ is the contact resistance between fillers [41]. The resistance of the filler material, R_f, is usually negligible compared to the resistance between conductive filler particles, $R_{f\text{-}f}$. The contact resistance can be defined as:

$$R_{f\text{-}f} = R_c + R_t \tag{2}$$

where R_c is the constriction resistance and R_t is the tunneling resistance [42]. The three sources of resistance in a conductive composite are illustrated in Figure 1-5. The constriction resistance is due to the flow of electrons being confined to a smaller contact area when travelling from one conductive filler to the next. It is dependant on the diameter of the contact area:

$$R_c = \frac{\rho_c}{d} \tag{3}$$

where ρ_c is the intrinsic filler resistivity and d is the diameter of the contact spot [27]. The constriction resistance can be minimized by increasing the contact area, and sintering [43]. In ECAs, the sintering of the conductive filler and the curing of the polymer matrix are accomplished during the same step. The tunneling resistance, R_t, represents the probability of an electron tunneling between neighbouring conductive fillers and depends on the distance between neighbouring fillers and the properties of the organic, insulating film, e.g. the polymer matrix and any remnant organic films on the conductive filler

formed during their fabrication [42]. Assuming a uniform, fixed insulating film thickness between conductive fillers, the tunneling resistance can be defined as:

$$R_t = \frac{\rho_t}{A_c} \tag{4}$$

where ρ_t is the tunneling resistivity and A_c is the contact area [44].

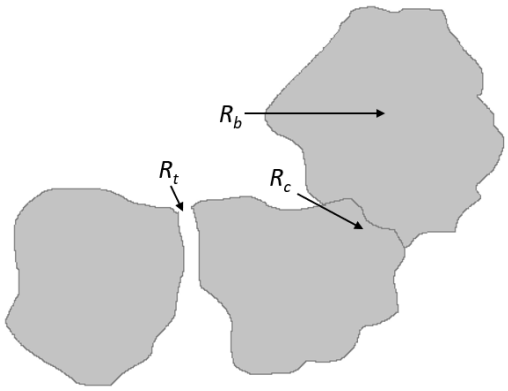

Figure 1-5: The three sources of resistance in a conductive composite, where R_b is the bulk resistance of the conductive filler, R_c is the constriction resistance and R_t is the tunneling resistance.

1.2.4 Alternate Conductive Fillers

Silver microflakes, as the name suggests, are micron-sized (~10 μm) flakes with thicknesses of a few hundred nanometers [45]. While they exhibit favourable electrical properties and are relatively low cost, networks of AgMfs are brittle, and the flakes lose contact with each other under mechanical strain. As will be shown in Chapter 2, commercial ECAs, which as mentioned above use AgMfs as the conductive filler, break and lose conductivity when subject to mechanical strain. They are thus not appropriate for use in FHE applications. Furthermore, as illustrated in Figure 1-3, the shape of flakes results in a high percolation threshold, which necessitates high concentrations to achieve conductivity. There is a trade-off with the filler concentration used. If it is too high, there is too little polymer adhesive, which results in poor adhesion strength. If it is too low, conductivity suffers. Some mid-point needs to be used and as such, both the adhesion strength and conductivity are lower than ideal. Conductivity also suffers because flakes do not sinter as well as nano-sized structures at the temperatures compatible with flexible substrates.

Due to the limitations of AgMfs, other nanostructures are being considered as conductive fillers for ECAs.

1.2.4.1 Carbon Nanotubes

Many studies have considered carbon nanotubes (CNTs) as a conductive filler in ECAs. They have excellent mechanically properties, being approximately 10 – 100 times stronger than steel at a fraction of the weight [46]. Also, due to their high aspect ratio, CNTs have a low percolation threshold, which allows them to achieve conductivity at a low fill fraction. Percolation thresholds below 1 wt% have been demonstrated experimentally [47], [48]. This allows for the use of more polymer adhesive and indeed, low fill fractions of CNTs have been shown to increase the adhesion strength of CNT-based ECAs [26].

However, CNT-based ECAs do not address the conductivity concerns of ECAs as they are not able to achieve as high of a conductivity as AgMf-based ECAs. Although the bulk resistivity of CNTs can be much lower than other materials, [26] unlike metallic fillers, CNTs cannot be sintered to reduce the junction resistance between CNTs. As such, the resistance of their networks is high. The lowest reported resistivity of pure CNT-based ECAs in literature is approximately 8.33 Ω·cm [23] while the resistivity of AgMf ECAs is on the order of 10^{-4} Ω·cm [23], [27], [49] and the resistivity of solder is approximately 2 x 10^{-5} Ω·cm [50]. Moreover, the fabrication of CNTs results in metallic and semiconducting CNTs, which are difficult to separate. Semiconducting CNTs are much less conductive than metallic ones and therefore, contribute little to the conductivity of the ECA.

1.2.4.2 Silver Micro- and Nanostructures

Different morphologies of silver have been investigated for their viability as a conductive filler for ECAs. Silver nanoparticles (AgNPs) were one of the first alternatives to AgMfs explored. While AgNPs do exhibit a lower percolation threshold than AgMfs [51], they cannot achieve as low of a resistivity due to the increased number of contacts and the smaller size of these contacts [35], [52]. The high number and smaller area of contacts may also make it more difficult for AgNP-based ECAs to maintain an electrical connection under mechanical strain. Another morphology of interest are silver hexagonal microsheets, which have a similar size and shape to AgMfs, but are smoother and straighter. This smooth surface allows them to achieve better contact with each other. Silver microsheet-based ECAs have demonstrated a bulk resistivity on the same order of magnitude as solder, 8 x 10^{-5} Ω·cm [53]. However, like AgMfs, they require a high fill fraction to achieve good conductivity. Silver microdendrites, which are a three-dimensional, branched microstructures, show a lot of potential as a conductive filler. They can achieve similar conductivities to AgMfs at a lower fill fraction. Due to their nanosized branches, they can be sintered at lower temperatures, as low as 80 °C, and their three-

dimensional structure may potentially maintain a better electrical connection under mechanical strain [54]. However, there is still a lot of work to be done before the synthesis of silver microdendrites is industry ready. Silver microdendrites also have a higher percolation threshold than other silver nanostructures.

1.3 Silver Nanowire ECAs

Silver nanowires (AgNWs) are one of the most promising conductive filler materials for ECAs due to their excellent mechanical and electrical properties. Nanowires are cylindrical-shaped nanostructures with typical diameters between 30 – 100 nm and lengths up to 200 μm. Because they are crystalline, the conductivity of AgNWs, ~0.8×10^5 S/cm, is comparable to the conductivity of bulk silver, 6.2 x 10^5 S/cm [55]. Unlike CNTs, overlapping AgNWs can be sintered to lower their junction resistance.

AgNWs are synthesized through a variety of chemical and physical processes but the most common and most industry viable approach is the polyol process [56]. The polyol process involves the reduction of an inorganic salt by a polyol in the presence of a capping agent [57]. In the presence of a seed, nanowires will form. In the case of AgNWs, silver nitrate is reduced by ethylene glycol in the presence of poly(vinyl pyrrolidone) (PVP) [58]. Originally, platinum seeds were used [55], but due to the cost of platinum, and the desire to simplify the process, a self-seeding process using silver nitrate has gained popularity [59]. The AgNW synthesis process is illustrated in Figure 1-6. In the initial phases of the reaction, silver decahedral nanoparticles are formed and as the reaction proceeds, these nanoparticles grow through Ostwald ripening [58]. PVP reacts more favorable with the newly formed {100} facets than the {111} facets promoting the anisotropic growth of the nanoparticles into nanorods and eventually nanowires. The presence of chloride ions in the solution helps facilitate the growth of AgNWs by stabilizing the AgNPs [57]. The polyol process does also create AgNPs but the AgNWs can easily be separated from the AgNPs through centrifugation [55]. The resulting nanowires have a pentagonal cross section and a 5-fold twinned crystal structure with sides bounded by {100} facets [58]. Their longitudinal axes align along the <110> direction.

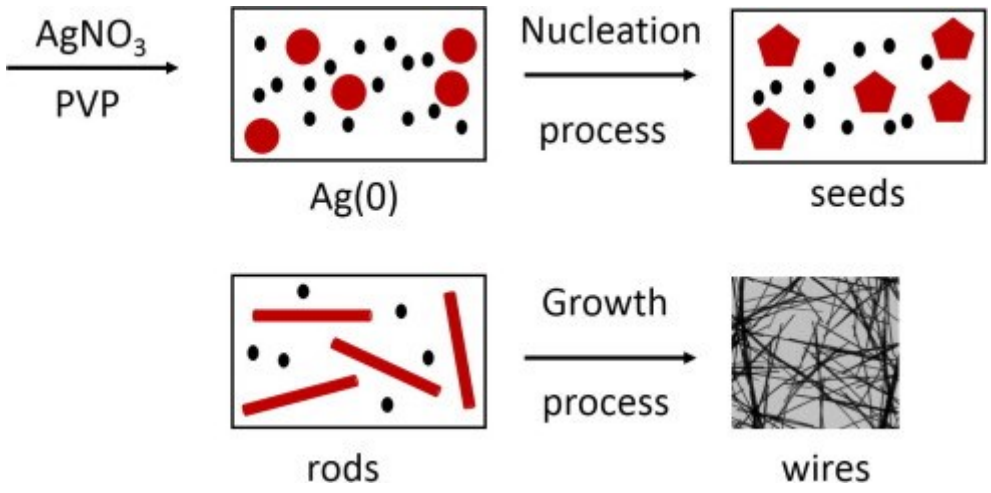

Figure 1-6: A schematic of the polyol process used to synthesize AgNWs, from [57]**. (Reprinted with permission from Elsevier).**

When used as a conductive filler in an ECA, AgNWs can address the conductivity, adhesion strength and flexibility concerns related to AgMf-based ECAs. To begin with, AgNW ECAs have already been demonstrated to have superior electrical properties over AgMf ECAs. Wu et al. showed that a 56 wt% AgNW ECA had better conductivity than a 56 wt% and even a 75 wt% ECA filled with 1 μm Ag particles [27]. And Wang et al. showed that at fill fractions of 55 and 65 wt%, AgNW ECAs perform better electrically than AgMf ECAs [33]. At these fills, the percolation threshold of NWs is certainly surpassed, and due to their small diameter, AgNW junctions sinter much better than flake-flake junctions. Wang et al. also showed that the higher surface area of AgNWs, compared to AgMfs, has a better interaction with the epoxy resin, resulting in a higher cross-linking density of the polymer matrix [33]. This increases the shrinkage of the epoxy resin, which imparts a compressive force on the nanowire junctions, reducing the contact resistance.

The lower percolation threshold of AgNWs allows for a lower metal fill and therefore, higher adhesive content, which in turn should lead to stronger adhesion. Even at equivalent fill fractions, Li et al. demonstrated that AgNWs ECAs have a higher shear strength than AgMf ECAs [60]. This was attributed to the larger surface area of the AgNWs, compared to the AgMfs, which can be wetted more easily by the epoxy resin. Furthermore, although the impact of AgNWs on the mechanical flexibility of ECAs has not been studied, AgNWs in transparent electrodes have been shown to be highly bendable and stretchable with minimal impact on conductivity [61]–[63]. The long reach of the AgNWs allows the conductive network to remain intact when bent or strained. In addition, the AgNW network, which is web-like with thin pathways and open space in between, can rotate and deform under mechanical

strain. Further, the pentagonal shape of polyol-synthesized AgNWs improves their yield strength compared to bulk silver [61].

As alluded to above, an additional advantage of AgNW is that because of to their smaller diameters, their junctions sinter at lower temperatures than AgMfs [33], [64]. This is due to the Gibbs Thomspon effect. If comparable conductivities to conventional ECAs are attainable at lower temperatures using AgNWs, more applications are open to the ECA. For instance, TPU, which has a greater mechanical flexibility than PET, is more sensitive to the processing temperature than PET. Paper and textiles are even more thermally sensitive.

Although these benefits are numerous, there are several limitations preventing AgNW ECAs from being adopted by industry. Commercially available AgNWs are approximately 40 – 50x more expensive than AgMfs, due to their synthesis process. This increases the raw material cost of the ECA even though in many cases less silver can be used. Secondly, AgNW agglomeration is an issue at higher filler fractions. And thirdly, the small nanowire diameter means a smaller contact area at overlapping nanowires, limiting conductivity.

1.4 Silver Nanowire Microflake Hybrid ECAs

The shortcomings of one conductive filler can be addressed by adding a second conductive filler, referred to as a secondary or auxiliary filler. The strengths of the auxiliary filler address and mask the weaknesses of the primary filler and vice versa resulting in an ECA with superior properties compared to one with either of the fillers individually [65]. Further, the ratio between the primary and auxiliary filler can be fined tuned to optimize the results. The auxiliary filler can be a different size [66], shape [49], [65], [67] or even material [37], [64], [68]. The auxiliary filler can be chosen to improve the conductivity, lower the percolation threshold and/or improve the mechanical properties depending on the application. The advantages of silver microflakes over silver nanowires include a lower cost, larger contact area [41] and lower oxidation rates while the advantages of silver nanowires include better mechanical and electrical properties, a lower sintering temperature [41], and a lower percolation threshold. By combining the two fillers in one ECA, the ECA will exhibit better electrical and mechanical properties while being lower cost and lightweight.

There have been several reports of silver nanowire/microflake hybrid ECAs. The silver nanowires bridge neighbouring silver microflakes creating an electrical connection between them and the silver microflakes act as junctions in the nanowire network [69]. Due to the large contact area provided by

the AgMfs, the small diameter/contact area between AgNWs is no longer a concern. The hybrid ECAs have been shown to have a lower percolation threshold and improved conductivity [67], [69], [70] compared to either pure Mf and pure NW ECAs, as shown in Figure 1-7. For the highest conductivity at a fixed total silver fill, there is an optimal ratio of silver nanowires to silver microflakes [71]. Above the optimal ratio, replacing more silver microflakes with silver nanowires results in agglomeration of the nanowires on the surface of the microflakes increasing the contact resistance and therefore, decreasing the conductivity. The optimal nanowire to microflake ratio is typically on the range of 20 to 30% of the total silver content [71], which means the majority of the filler is the AgMfs, alleviating some of the cost concerns associated with AgNWs. At these ratios of AgNWs to AgMfs, agglomeration of the AgNWs is not a concern. As aforementioned, the larger contact area provided by the AgMfs at junctions in the network further helps improve the conductivity of the ECA.

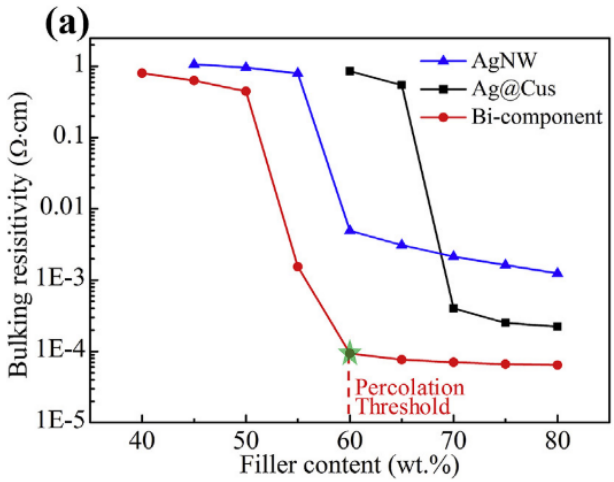

Figure 1-7: The conductivity of a silver nanowire ECA (blue), a silver-coated copper microflake ECA (black) and a hybrid ECA (red) using the two fillers, from [64]**. The hybrid ECA exhibits the lowest resistivity and percolation threshold. (Reprinted with permission from Elsevier).**

Despite the evidence of improved electrical properties, there is still more that needs to be understood about silver nanowire microflake hybrid ECAs before they are ready for commercialization in FHEs. First, although their size and aspect ratio are the key reasons for the advantages of NWs over Mfs, no one has studied the effect of diameter and length on the properties of NW or NW/Mf hybrid ECAs. Second, one of the most common methods for mixing an ECA is ultrasonication [33], [35], [67], [68], which has previously been shown to break AgNWs, degrading their performance [72]. The impact of the ultrasonication on the properties of the ECA needs to be understood and will be addressed in this thesis. Last but not least, as the focus of commercial ECAs has been as a solder replacement, which is

typical used on mechanically rigid PCBs, the flexibility of ECAs has been neglected. Due to the growing demand for ECAs in FHEs, which are subject to bending and straining, I study for the first time how the addition of NWs to flake-only ECAs can improve their ability to bend and stretch and their ability to retain these improved properties over many cycles.

1.5 Thesis Organization

The purpose of this work is to investigate the application of silver nanowires as a secondary filler to silver microflakes in a controlled manner to improve the mechanical and electrical properties of ECAs for FHEs. The key parameters that will be focused on are the flexibility, conductivity, and adhesion strength of the ECA, with flexibility taking priority. Chapter 2 will establish the materials and methodologies used in this work as well as establish a baseline by investigating the properties of pure silver microflake ECAs and a commercial ECA. Chapter 3 investigates the addition of the silver nanowires into the ECA fabrication process and addresses potential obstacles, such as damage to the silver nanowires from ultrasonication. It investigates the influence of the morphology of the nanowires on the properties of the ECA to determine the optimal configuration. Chapter 4 demonstrates the real-world viability of the optimal ECA by fabricating an FHE device – a light emitting diode integrated on a flexible substrate. The device is compared against an identical device fabricated using the flake-only ECA. Finally, Chapter 5 summarizes the key findings of this work, and discusses future work that needs to be done before hybrid silver nanowire microflake ECAs are ready for market.

Chapter 2
ECA Preparation and Characterization

In this chapter, a description of how I fabricated a pure microflake ECA in-house is first described. This procedure will be the basis of all ECA fabrication in this thesis, with some modifications taken for the addition of nanowires (to be described in Chapter 3). Afterwards, in Section 2.2, the methodologies used to characterize all ECAs in this thesis are described. The characterization results of my microflake ECA and the commercial ECA are presented in Section 2.3 as a baseline against which the nanowire/microflake ECAs in future chapters will be compared.

2.1 Fabrication of Microflake ECA

2.1.1 Materials

Silver microflakes (AgMfs) with a nominal diameter of 10 μm were used as the conductive filler. The epoxy resin Bisphenol A diglycidyl ether (DGEBA) was used as the polymer matrix and it was cured using Triethylenetetramine (TETA). The DGEBA, TETA, and AgMfs were purchased from MilliporeSigma (Burlington, Massachusetts, USA) and used as received. The DGEBA slowly crystallizes over time and was periodically heated to 50 ℃ to reverse crystallization as directed by the manufacturer.

2.1.2 Fabrication

The AgMf samples were prepared using the following steps. It is a modified version of the procedure given in [37]:

1. The AgMfs were weighed based on the desired fill fraction of 60 wt% and transferred to a centrifuge tube.

The mass/fill fraction of the conductive filler can be calculated using:

$$w_{\text{filler}} = \frac{m_{\text{filler}}}{m_{\text{total}}} \text{x } 100\ \% \tag{1}$$

where w_{filler} is the fill fraction in wt%, m_{filler} is mass of the conductive filler, and m_{total} is the total mass of the ECA, i.e., the resin, hardener, and conductive filler combined. The mass of the solvent is not included as it is removed during curing. The fill fraction was fixed at 60 wt% as this is approximately the percolation threshold for AgMfs (the exact percolation threshold depends on the size, size

distribution, and shape of the flakes) [73]. This allows a good conductivity to be achieved, while keeping the amount of conductive filler used minimal. Using less filler reduces the cost and weight of the ECA and improves the mechanical properties as excessive filler degrades the mechanical properties of the polymer matrix. Adding more filler past the percolation threshold has a diminishing return on improving the conductivity.

2. 50 µL of ethanol was added to the centrifuge tube and vortex mixed for 10 seconds.

This solvent is used to facilitate mixing. It is briefly mixed with the conductive filler prior to adding the resin as without doing so, the resin would displace the solvent when it is added, making it harder to mix.

3. 120 mg of DGEBA (epoxy resin) was added to the centrifuge tube. The epoxy resin was heated for 10 minutes at 60 °C prior to adding it.

The amount of resin used was fixed as this allowed the amount of hardener added to be fixed too. For a fixed wt%, the total amount of conductive filler added is fixed too. The purpose of heating the epoxy resin prior to adding it is twofold. First, it reduces the viscosity of the resin making it easier to work with when weighing it and easier to mix. Secondly, the resin slowly crystallizes over time at room temperature. Heating the resin reversed any crystallization that had taken place.

4. The mixture was ultrasonicated for 90 seconds and then vortex mixed for 30 seconds.

The combination of ultrasonication and vortex mixing facilitated a good dispersion in the resin. These short mixing times were used as when silver nanowires (AgNWs) are incorporated into the process in subsequent chapters, long mixing times can be problematic (as will be discussed in Chapter 3).

5. 16 µL of TETA (hardener) was added to the mixture. The mixture was vortex mixed for an additional 2 minutes.

The hardener and resin were mixed at a ratio of 13:100 by weight, respectively. Due to the small amount volume of hardener required, it was easier to convert the required weight to a volume and measure it using a pipette.

6. The ECA was printed onto the appropriate test coupon using stencil printing.

The ECA was printed onto an 89 µm thick film of thermoplastic polyurethane (TPU) (ST-604, Bemis Associates Inc.) for flexibility, conductivity, and microscopy measurements, and onto aluminum 5052 for shear strength measurements. The plastic liner was removed from the TPU prior to printing and the

substrate was cleaned with isopropanol alcohol. The aluminum was cleaned with acetone prior to printing.

The stencil, along with a printed sample, is shown in Figure 2-1. The stencil consists of a 12.7 cm x 17.78 cm x 50.8 μm thick, stainless-steel foil mounted in a 20.32 cm by 25.4 cm frame for hand printing. Once the ECA is transferred onto the metal foil, a squeegee (Speedball 4491, 65 durometer) is passed over it to transfer the pattern onto the substrate. The print direction aligned with the direction of the applied strain during the flexibility testing.

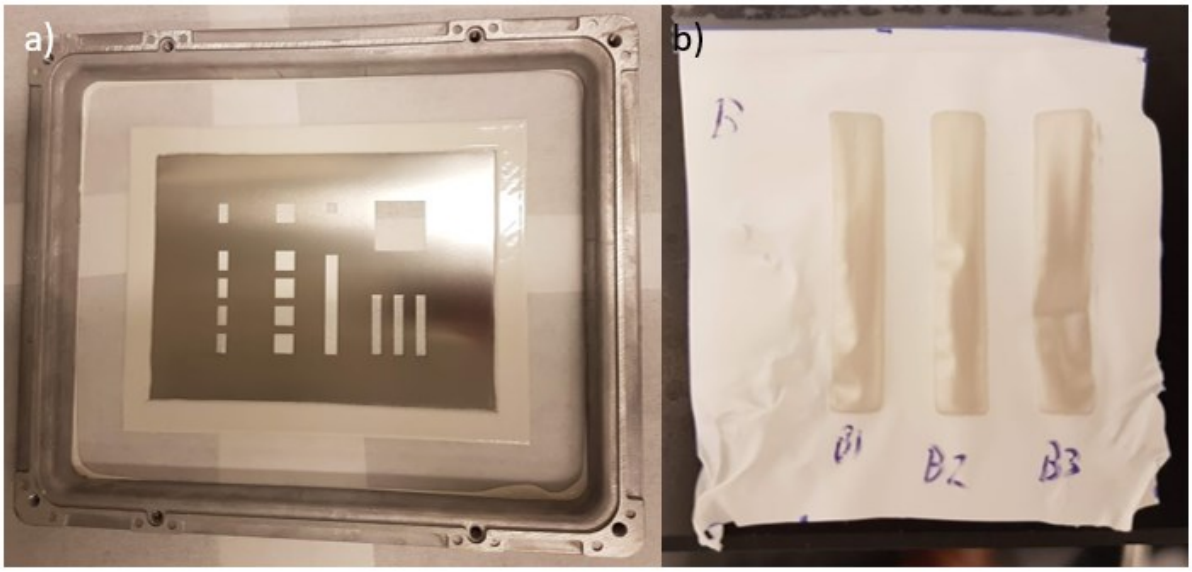

Figure 2-1: a) The stencil used for printing the ECA samples. The pattern in the bottom right was used for printing samples for flexibility and conductivity tests, while the pattern in the top right was used for printing samples for single-lap shear tests. b) A printed and cured sample for flexibility tests.

7. Precure the ECA for one hour at 60 °C.

The purpose of this step is to remove any residual solvent. It is done at a lower temperature and on a hot plate, as opposed to a vacuum oven, to slowly remove the residual solvent. Removing it too quickly could leave voids in the ECA, weakening its mechanical properties.

8. Cure the ECA for two hours at 150 °C.

After the residual solvent is removed in the previous step, the temperature of the hot plate is ramped to 150 ℃ to fully cure the epoxy. This step also helps sinter the conductive filler, which improves the flake-flake contacts and thus overall electrical properties of the ECA.

2.1.3 Commercial ECA Deposition

The commercial ECA used as a reference was the 8330S epoxy produced by MG Chemicals (Burlington, Ontario, Canada). The two-part epoxy was mixed according to the vendor's specifications:

1. 1.1 part of mixture A and 1 part of mixture B were weighed and mixed thoroughly using a spatula.

As recommended by the vendor, the two parts were measured by weight, as opposed to by volume as less than 1 mL was being used. The ECA was mixed in the weighing boat the two parts were measured out in.

2. The ECA was deposited and cured using steps 6 - 8 from Section 2.1.2.

According to the product's specification sheet, the ECA could be cured at as low as 65 °C for two hours. However, the same temperature and duration used for the AgMf samples was used here, which is higher and longer (when including the precure) than the spec sheet, to ensure a fair comparison with the AgMf samples (since higher temperatures and longer cure durations typically lead to improved conductivities).

2.2 Characterization

2.2.1 Electrical Conductivity Measurements

Conductivity measurements were taken using a four-point probe (T2001A3-US, Ossila Ltd). A four-point probe was used as it eliminates contact resistance. As the name suggests, four probes, with equal spacing, are applied to the sample as shown in Figure 2-2. The two outer probes apply a current to the sample and the voltage across the inner probes is measured. The voltmeter has a high impedance, thus preventing any current from flowing through it. The sheet resistance can then be calculated using [74]:

$$R_s = C \cdot \left(\frac{\pi}{\ln 2}\right)\frac{V}{I} \tag{2}$$

where R_s is the sheet resistance, V is the voltage across the inner probes, I is the applied current and C is a geometric correction factor based on the sample dimensions and probe spacing.

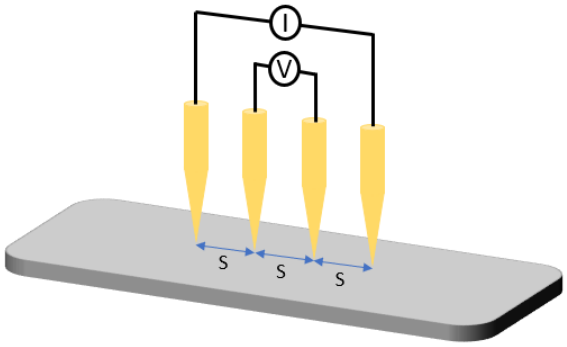

Figure 2-2: A four-point probe schematic. *S* is the spacing between the probes.

From the sheet resistance, the resistivity can be calculated using [74]:

$$\rho = R_s \cdot t \tag{3}$$

where ρ is the resistivity and t is the thickness of the sample. In this work, t = 50.8 µm for all samples (the thickness of the stencil used).

Resistivity measurements were taken at three points along the length of the sample to account for variations due to the hand-printing. The lowest resistivity measurement, usually the measurement at the center of the sample, was taken as representative of the whole sample as it is believed this is the resistivity achievable with an automated process. The reported mean resistivity is the mean of the best 3 - 6 samples prepared, depending on the study and number of samples prepared.

2.2.2 Single-lap Shear Tests

A single-lap shear test measures the maximum tensile load an adhesively bonded joint can withstand before breaking (shearing) [75]. It is a measure of the bond strength of the adhesive and is commonly used due to its simplicity and low cost. The tests were conducted according to the ASTM D1002 standard using an 810 Material Test System equipped with 647 Hydraulic Wedge Grips. The tests were carried out with a constant displacement rate of 1.3 mm/s and the samples had an overlap area of 12.7 mm by 25.4 mm. The sample geometry is shown in Figure 2-3. The samples have a spacer on either end, a 25.4 mm by 25.4 mm piece of aluminum, to align them within the wedge grips. Aluminum 5052 was used as the substrate as this is the material for which the single-lap shear strength of the commercial ECA is known.

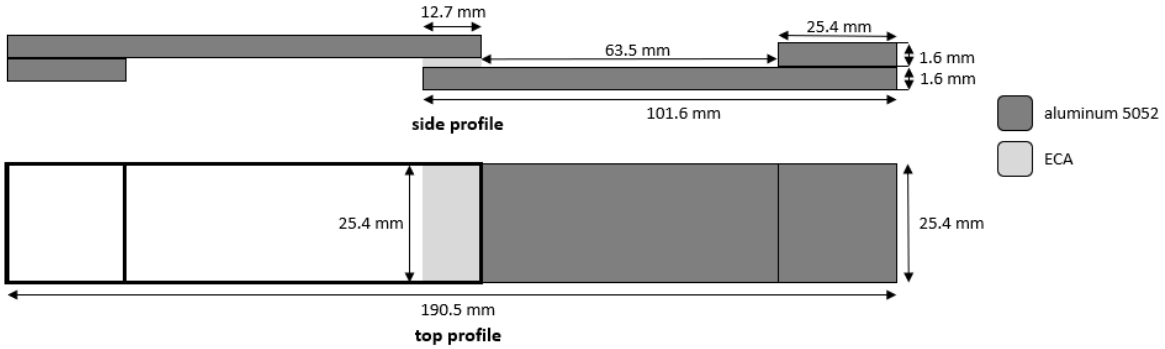

Figure 2-3: The single-lap shear strength sample geometry based on the ASTM D1002 standard.

The test gives the maximum load applied before the failure. From this value, the shear strength of the ECA can be calculating using:

$$\tau = \frac{F}{A} \tag{4}$$

where τ is the shear strength of the sample, F is the maximum load applied and A is the cross-sectional area, i.e. the area of the overlap.

2.2.3 Flexibility Tests

Strain cycling and maximum elongation tests of the ECAs were conducted using a linear stage (Zaber Technologies X-LHM150A). The setup, with a sample ready to be tested, is shown in Figure 2-4. One end of the sample was clamped at the end of the axis and the other end of the sample was clamped onto the linear stage and would strain/relax the sample as the linear stage moved. The resistance of the sample was measured via a digital multimeter (SIGLENT Technologies SDM3045X) attached to the clamps holding the sample. The speed of the linear stage was set at 1 mm/s and the initial length of the sample between the clamps was 1 cm. For the flexibility measurements, 3 cm x 0.5 cm x 50 µm strips of the ECA were stencil printed onto a 5.08 cm x 3.81 cm x 89 µm piece of TPU.

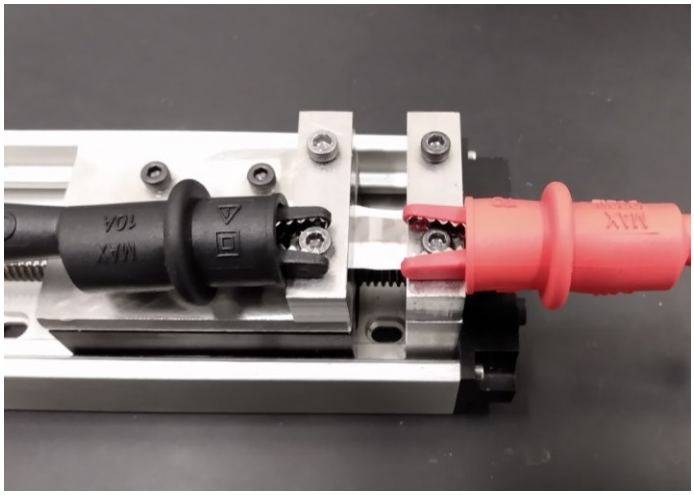

Figure 2-4: The flexibility test setup. The clamp on the right is fixed, while the clamp on the left is attached to the linear stage and moves freely.

2.2.3.1 Test Automation

To coordinate the strain cycling and electrical measurements, custom software using the Python™ programming language was written. This allowed precise control over which points in the strain cycle electrical measurements were taken and how the strain cycling occurred. Zaber Technologies and SIGLENT Technologies both offer programs to control their products, the linear stage and digital multimeter respectively, but these programs cannot communicate with each other and therefore cannot coordinate the tests. The linear stage was controlled using the Zaber Motion Library, by Zaber Technologies, which provides an application programming interface (API) for communicating with the linear stage. The digital multimeter was controlled using the virtual instrument software architecture (VISA) API. The Keysight IO Libraries Suite 2021 was used as the VISA library and the PyVISA Python™ package was used to interact with the VISA library.

The custom software begins by connecting to the instruments, and setting the linear stage speed to 1.0 mm/s. After waiting a fixed amount of time, it begins the strain cycling. It stretches the sample to the desired strain, usually 30%, and waits 300 ms for the digital multimeter to stabilize (including determining the measurement range) before taking the resistance measurements. It then takes the desired number of measurements, waiting one second between measurements. It then relaxes the sample, again waiting 300 ms for the digital multimeter to stabilize and takes the same number of resistance measurements. This is repeated for the desired number of cycles, usually 100 or 250. After the strain cycling is completed, the software continues to take resistance measurements for ten minutes,

with one second between measurements, to analyze the recovery behaviour of the sample. The software then saved the data and closed the connections.

For maximum elongation measurements, where the sample is subjected to an increasing amount of strain until it loses conductivity, the software follows a similar procedure, except it skips the relaxation step. The sample is strained by the desired step-size, usually 5%, resistance measurements are taken, and the software increases the strain again by the step-size. This is repeated until the desired strain is reached. Afterwards, the sample is relaxed, and the software concludes as before, taking resistance measurements for ten minutes.

2.2.4 Scanning Electron Microscopy

Scanning electron microscopy (SEM) images were taken using a Schottky Field Emission Scanning Electron Microscope (SU5000, Hitachi High-Tech Corporation) to observe factors such as the dispersion of the conductive filler, possible damage to the filler during mixing, and changes in the ECA after strain cycling. In the case of the hybrid ECAs, the interaction between the silver nanowires and microflakes was of interest. To prepare a sample for SEM, a strip of ECA, approximately the length of the SEM stub, was cut from a flexibility sample, either before or after straining, and mounted onto the SEM stub using carbon tape.

2.3 Baseline Results

To establish a baseline against which the hybrid silver nanowire microflake ECAs (in Chapters 3 and 4) can be tested, 60 wt% pure AgMf and commercial ECA samples were prepared and characterized.

2.3.1 Conductivity

As shown in Figure 2-5a), the mean resistivity of the commercial ECA was 9.3×10^{-5} Ω·cm and the mean resistivity of the 60 wt% pure AgMf samples was 1.9×10^{-3} Ω·cm. The resistivity of the 8330S commercial ECA is lower than the 7.0×10^{-4} Ω·cm specified by the vendor, MG Chemicals, due to the higher curing temperature. The resistivity of the 60 wt% AgMf reflects values seen in literature for similar curing conditions and composition [49].

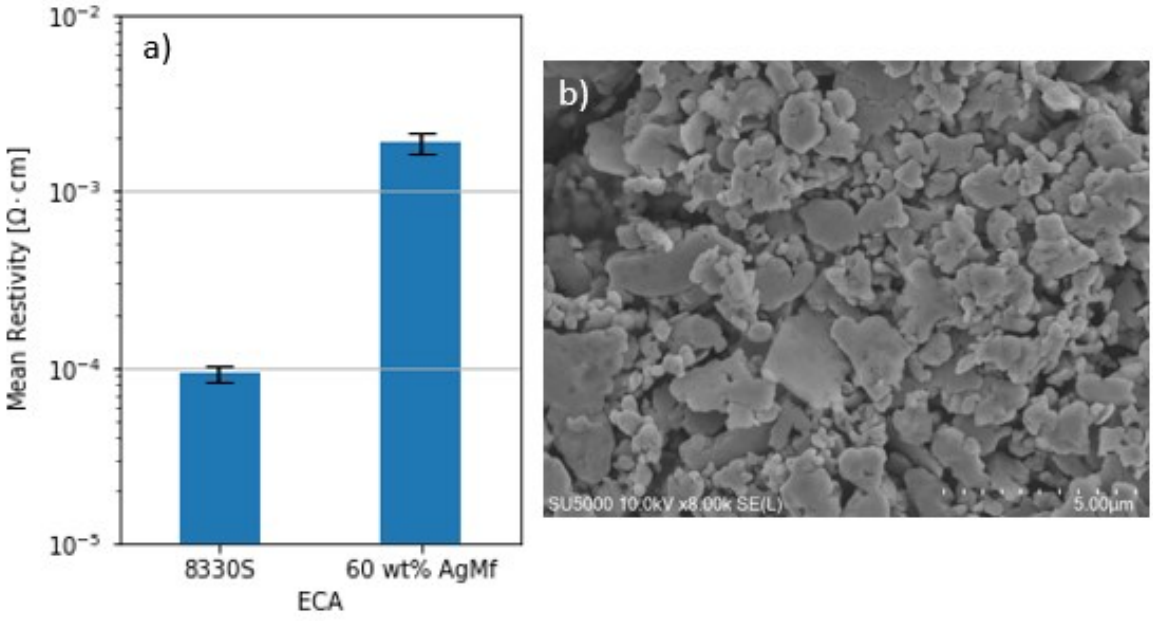

Figure 2-5: a) The resistivity of the 8330S commercial ECA and the in-house 60 wt% AgMf ECA. b) An SEM image of an in-house 60 wt% pure AgMf ECA showcasing the continuous conductive pathway formed by the AgMfs for electrons to travel through.

The SEM image of the in-house 60 wt% pure AgMf ECA, shown in Figure 2-5b), confirms the expected behaviour of conventional AgMf ECAs. Above the percolation threshold, there is a continuous network of AgMfs in contact that allows current to flow through the insulating polymer matrix. The main source of resistance is the constriction resistance, i.e. the resistance between neighbouring AgMfs, as the bulk resistance of silver is low and the electrons do not need to tunnel between fillers when the fillers are in contact.

2.3.2 Flexibility

The flexibility results for strain cycling at 30% strain for 100 cycles are shown in Figure 2-6. The 8330S samples broke during the first cycle and are thus not shown on the graph. There were large ruptures in the ECA visible by eye and the samples did not recover after 10 minutes after the conclusion of the cycling. The best performing sample had a resistance increase of over 17,000x after the first cycle. This is expected as the current focus of commercially available ECAs is solder replacement and therefore, flexibility is not a priority. The 60 wt% AgMf sample peaked at an increase of 25x during the 100th cycle and then dropped to 14x during relaxation. After 10 minutes of relaxation, the resistance of the sample recovered to 5x the original resistance. Small cracks were visible by eye along the sides of the

ECA but there were no ruptures. In Figure 2-6b), the results of straining a 60 wt% AgMf sample to 150% are shown. The sample failed, defined as the resistance increasing to over 1 MΩ (essentially an open circuit), after 75% strain. After releasing the strain, the sample regained conductivity but there was plastic deformation of the substrate. After 2 minutes of relaxation, the resistance recovered to 7.1x the initial resistance before straining.

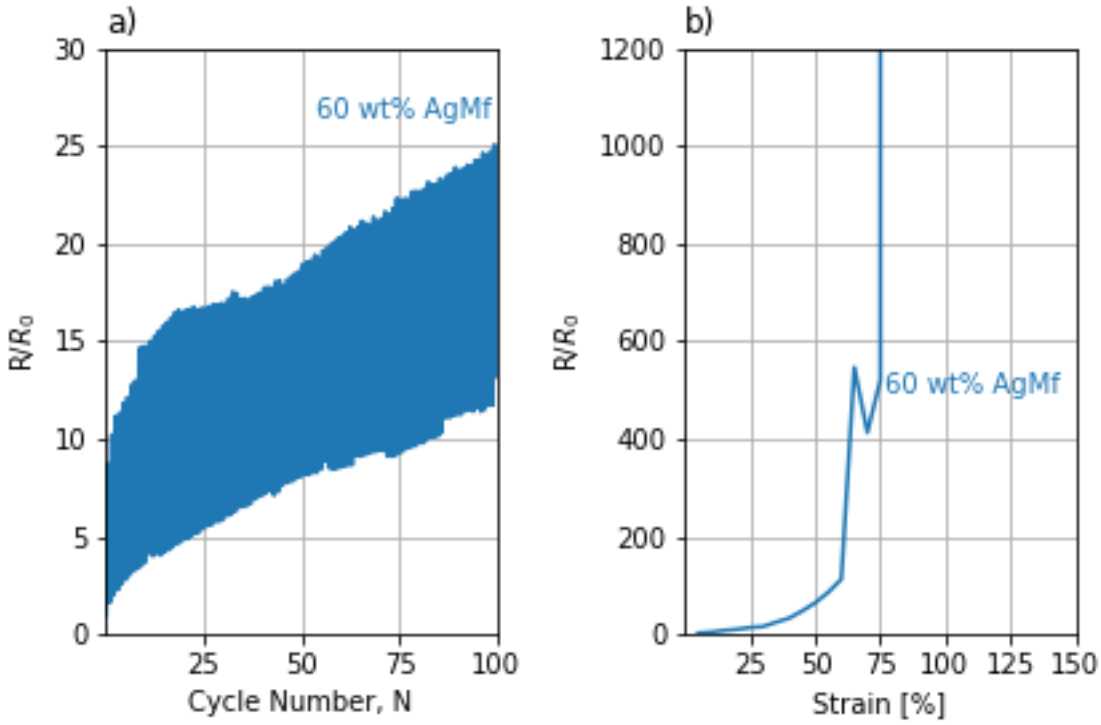

Figure 2-6: The a) strain cycling (100 cycles to 30%) and b) max elongation results for the baseline 60 wt% pure AgMf ECA. The commercial ECA samples are not shown as they broke during the first cycle of the strain cycling.

SEM images of a sample after strain cycling at 30% over 100 cycles, one of which is shown in Figure 2-7a), reveal the formation of microscopic cracks in the ECA. The repeatedly applied strain evidently damages and breaks some of the conductive pathways formed by the conductive filler, reducing the number of pathways available for the electrons to travel through, thereby increasing the resistance. During relaxation, some of these pathways are reformed (the flakes are in contact again) lowering the resistance. A similar structure is seen in Figure 2-7b), a sample that was strained to failure (75% strain). In this case, the cracks completely severed the electrical connection.

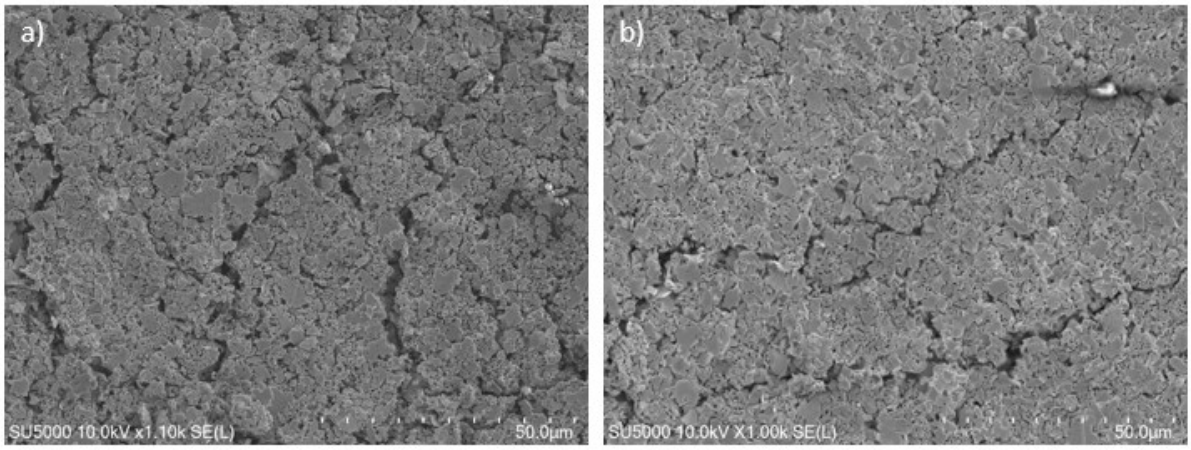

Figure 2-7: SEM images of an in-house, 60 wt% pure AgMf ECAs after a) strain cycling to 30% for 100 cycles and b) straining to failure (75%).

2.3.3 Singe-Lap Shear Strength Tests

The single-lap shear strength test results are shown in Figure 2-8. The shear strength of the commercial ECA was approximately 5.0 MPa, higher than the reported 2.6 MPa by the vendor due to the higher curing temperature. The shear strength of the 60 wt% AgMf ECA was approximately 6.0 MPa. This is resembles the approximately 5.0 MPa reported in literature for this composition and curing conditions [37]. The discrepancy is from the difference in substrates, aluminum 5052 vs copper clad FR-4. The samples failed both adhesively (adhesive delaminated from the substrate) and cohesively (adhesive ripped apart).

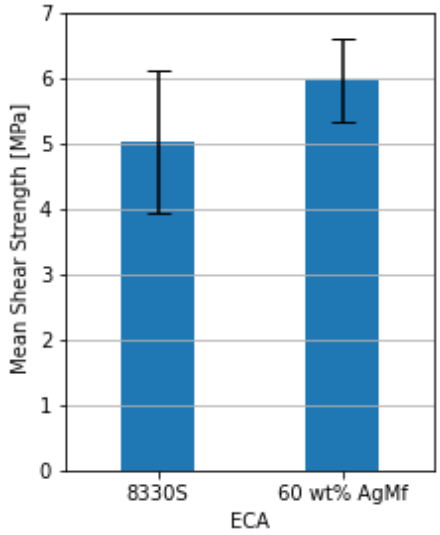

Figure 2-8: The single-lap shear strength test results of the commercial and in-house 60 wt% AgMf ECAs.

2.4 Conclusion

In this chapter, the materials, fabrication procedure and characterization methods of pure AgMf and commercial ECAs were presented. The fabrication procedure was validated by preparing in-house, 60 wt% AgMf ECA samples and comparing them to literature and the commercial 8330S ECA. As expected, the conductivity of the 8330S was superb, surpassing the 60 wt% AgMf ECA by an order of magnitude as conductivity is currently the focus of the ECA market. However, the 8330S ECA showed poor flexibility results, losing conductivity while being strained to 30% and thus it is unsuitable for use in flexible device applications. The AgMf ECA's resistance increased 25x during the 100^{th} cycle at 30% strain, and lost conductivity after being strained beyond 75%. The shear strength of the two ECAs was comparable at 5.0 MPa and 6.0 MPa for the 8330S and 60 wt% AgMf ECA, respectively.

Chapter 3
Hybrid Silver Nanowire/Microflake ECA Optimization

In this chapter, I first present the modified fabrication procedure to incorporate nanowires into nanowire/microflake hybrid ECAs. Key steps in the procedure, relevant to nanowires, will be studied and optimized. Afterwards, the impact of nanowire/microflake concentration ratio and morphology of the nanowires on the properties of the hybrid ECA will be studied. The results of the investigations in this chapter will be compared against the baseline ECAs from Chapter 2.

3.1 Fabrication of Hybrid Nanowire/Microflake ECAs

3.1.1 Materials

Silver nanowires (AgNWs) were purchased from Novarials Corporation (Woburn, MA) and used as received. The various AgNW series purchased, along with their properties, are listed in Table 3-1. The name denotes the medium, diameter and length of the AgNWs. The prefix, A or B, denotes whether the AgNWs arrive dispersed in a solvent or as a wet powder, respectively, the digits denote the average diameter of the AgNWs, in nm, and the suffix, SL, UL or none, denotes the length series, short length, ultralong or standard, respectively. In a hybrid sample, the AgNW to AgMf ratio is a weight ratio. For instance, a 1:4 sample contains 4x as many AgMfs by weight as AgNWs, i.e., the AgNW fill is 20% of the total silver content.

Table 3-1: The AgNWs purchased from Novarials for testing.

Name	Diameter [nm]	Length [µm]	Aspect Ratio	Medium
A30SL	30	5	167	10 mg/mL in ethanol
A30	30	30	1000	10 mg/mL in ethanol
-	30	150	5000	10 mg/mL in ethanol
A50	50	40	800	10 mg/mL in ethanol
A70	70	50	714	10 mg/mL in ethanol
A70UL	70	150	2143	10 mg/mL in ethanol
A100UL	100	150	1500	10 mg/mL in ethanol

B45	45	10	222	Wet powder
B100	100	10	100	Wet powder

The diameter and length values showed in Table 3-1 are the specifications provided by the manufacturer. Although the stated diameter is the average diameter of the nanowires, the length value is more indicative of the length of the longest nanowires in the series. SEM measurements performed by our group of the 30 nm diameter AgNWs reveal average lengths of 2.7, 27 and 88 μm, respectively for the A30SL, A30 and A30UL series [76].

3.1.2 Fabrication

Prior to Step 1 from Section 2.1.2, the following additional steps were taken to incorporate AgNWs received in solution into the hybrid ECA:

1. The amount of AgNWs, based on the desired fill fraction (total silver content = 60 wt%) and NW:Mf ratio, were centrifuged for 10 minutes.

This step is taken as the AgNWs need to be removed from their solvent. The excess solvent would prevent the ECA from mixing properly, plus the resulting viscosity would be too low to print the ECA.

2. The excess solvent was decanted and the AgNWs were combined into a new, clean centrifuge tube.

The AgNW solution had to be distributed among more than one centrifuge tube for centrifuging, and so, after decanting the solution, were combined into one centrifuge tube before moving onto the next steps.

3. The remainder of the procedure continues with Step 1 from Section 2.1.2 where the AgMfs are added to the same centrifuge tube as the AgNWs.

The following steps were taken for AgNWs in wet powder form:

1. The AgNWs were weighed based on the desired fill fraction (total silver content = 60 wt%) and NW:Mf ratio and transferred to a centrifuge tube.

The wet powder AgNWs could then be processed similarly to the AgMf powder.

2. Continue with Step 1 from Section 2.1.2 where the AgMfs are added to the same centrifuge tube as the AgNWs.

3.2 Mixing Optimization

One important consideration for the preparation of AgNW/AgMf hybrid ECAs is the sensitivity of the AgNWs to the processing conditions. AgNWs are long, thin one-dimensional nanostructures and therefore, need to be handled with greater attention. For instance, ultrasonication is required to disperse the conductive filler in the epoxy resin, but long ultrasonication times have been shown to damage and even break AgNWs [72].

3.2.1 Ultrasonication Study

To determine the optimal ultrasonication time, 1:6 A30UL (30 nm diameter, 150 µm length) AgNW/AgMf hybrid ECAs were prepared using different ultrasonication times: 1.5, 5, 10 and 20 min. A30UL AgNWs were chosen due to being long and thin, compared to the other AgNWs, which should make them more susceptible to damage during ultrasonication, thus highlighting the results. The results of the study are shown in Figure 3-1.

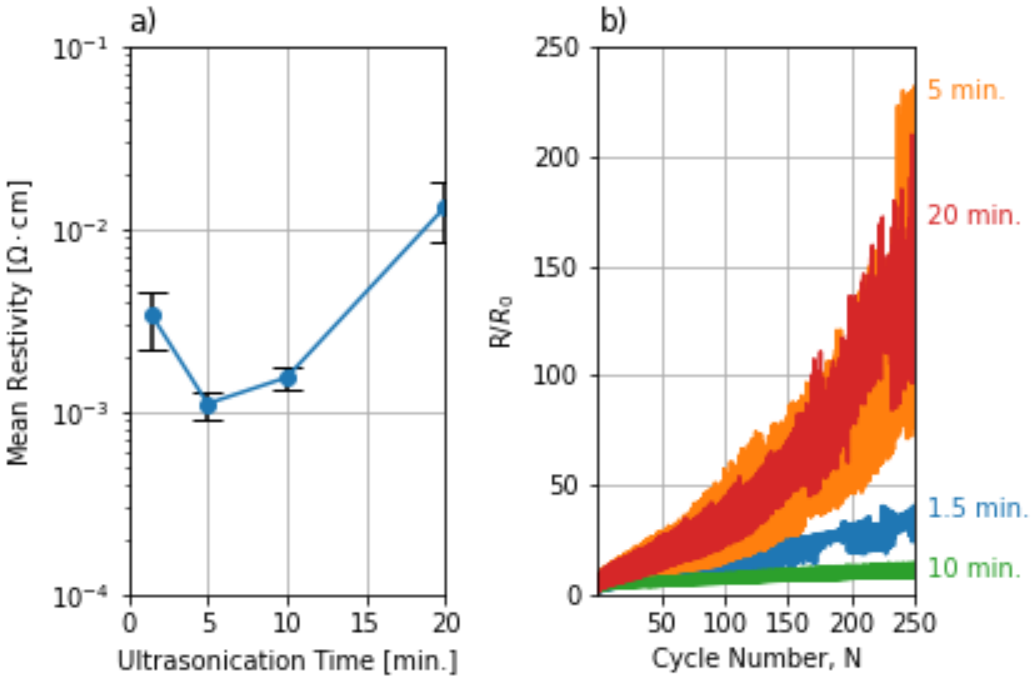

Figure 3-1: 1:6 A30UL AgNW/AgMf hybrid ECAs processed using different ultrasonication times: (a) their resistivity and (b) resistance change during flexibility measurements at 30% strain over 250 cycles.

It can be seen in Figure 3-1a) that there is an improvement in resistivity from 1.5 min. to 5 min. of sonication time. Further increases in sonication time, past 5 min., increases the resistivity. The resistivities of the 5- and 10- min. samples are similar at 1.1 x 10^{-3} and 1.6 x 10^{-3} Ω·cm, but increases by an order of magnitude at 20 min. The flexibility results are shown in Figure 3-1b). The sample sonicated for 10 min. showed the best flexibility. The resistance of the 10 min. sample increased 14x during the 250th cycle and recovered to 8.5x during relaxation. After 10 min. of recovery, the resistance decreased to 4.7x the initial resistance. Based on the conductivity results and SEM images (Figure 3-2), it is believed that the flexibility result of the 5 min. samples in Figure 3-1b) is an anomaly and they should instead show a flexibility improvement over the 1.5 min. samples. The anomaly could be due to issues with the test setup, sample/substrate preparation or a number of other factors. It is not clear whether the flexibility would be better or worse than the 10 min. sample.

During ultrasonication, there are two competing mechanisms with counteracting results. The first is the beneficial dispersion of the conductive filler(s) in the epoxy resin and is the purpose behind the ultrasonication step. A good dispersion of the conductive fillers will facilitate the formation of the conductive pathways through the polymer matrix and will improve the flexibility of the ECA. The second is detrimental damage to the nanowires. It has been noted by others that sonication can cause nanowires to break [72], which severs or impedes conductive pathways. The damage also introduces other defects which decrease conductivity [77] .

From the SEM images (Figure 3-2), and the conductivity and flexibility results (Figure 3-1), the dispersion of the conductive fillers is the dominant mechanism in the first phases of ultrasonication. In Figure 3-2a), a sonication time of 1.5 min. was used and AgNWs clumps are visible. These clumps are gone and a good dispersion of AgNWs is observed in Figure 3-2b), where a sonication time of 10 min. was used. This dispersion and separation of the clumps explains the improvement in conductivity and flexibility shown in Figure 3-1. There is some slight damage to the AgNWs at 10 min, with some “L”-shaped AgNWs visible, which explains the slight decrease in conductivity from 5 min. to 10 min. From 10 min. onwards, the ultrasonication primarily works to damage the AgNWs. At 20 min., shown in Figure 3-2c), there is substantial damage to the AgNWs with some AgNWs bent at large angles and “V”-shaped AgNWs seen.

Based on these results, the optimal ultrasonication time is somewhere between 5 to 10 min. dependent on the flexibility of the 5 min. samples.

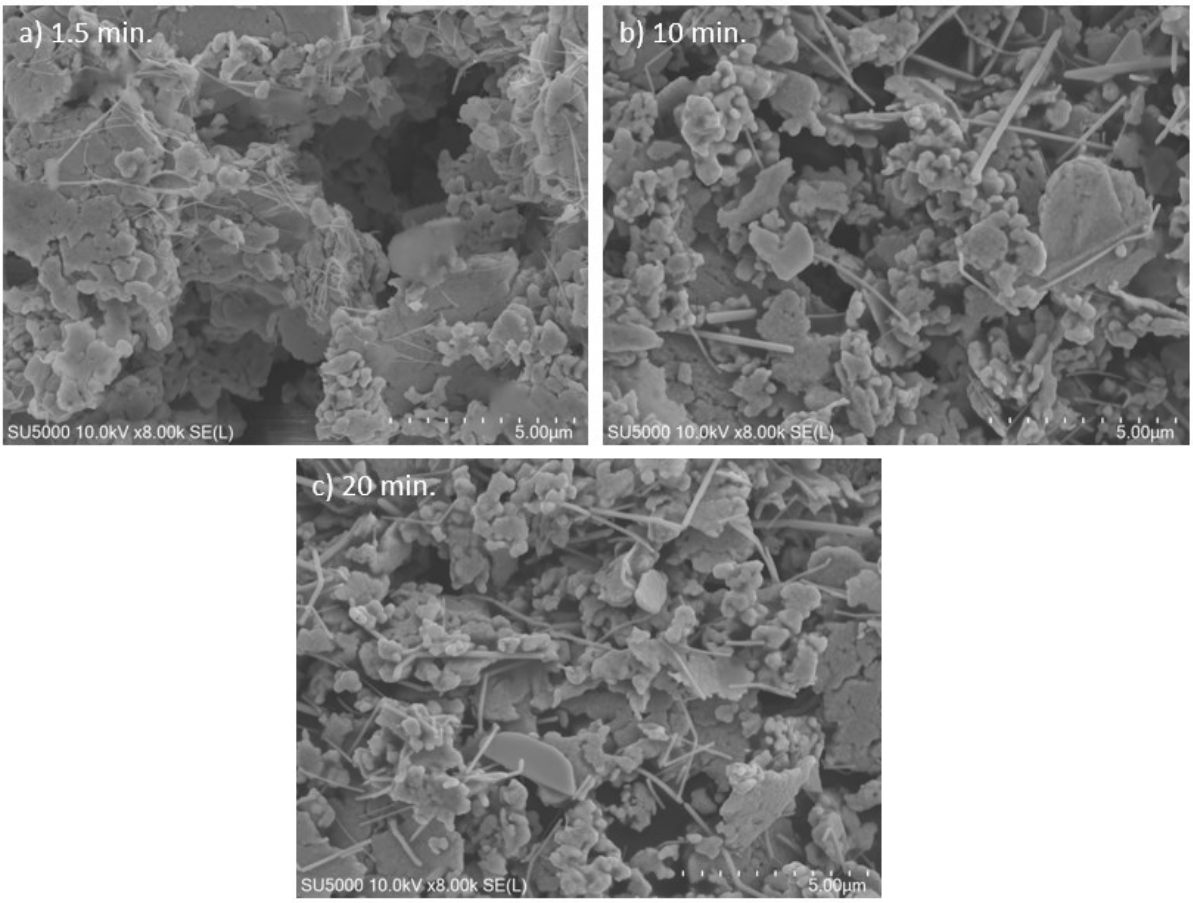

Figure 3-2: SEM images of 1:6 A30UL AgNW/AgMf hybrid ECA samples prepared using ultrasonication times of a) 1.5 min. b) 10 min. and c) 20 min.

3.2.2 Vortex Mixing Study

In addition to ultrasonication, the samples are subsequently mixed with a vortex mixer which also has the potential to further damage and/or break the nanowires. To investigate this, two 1:6 A30UL AgNW/AgMf hybrid ECAs were prepared using different vortex mixing times after adding the hardener: 90 seconds, and 120 seconds. The flexibility measurements are shown in Figure 3-3. The sample that was vortex mixed for 1.5 min. showed a resistance increase of 14x during the 250th strain cycle, while the sample that was vortex mixed for 2 min. showed an increase of 28x during the 250th cycle. The samples recovered to 4.7x and 5.1x after 10 minutes of relaxation, respectively. This suggests that prolonged mixing damages the nanowires. For this reason, 90 seconds was chosen as the optimal vortex mixing time after adding the hardener.

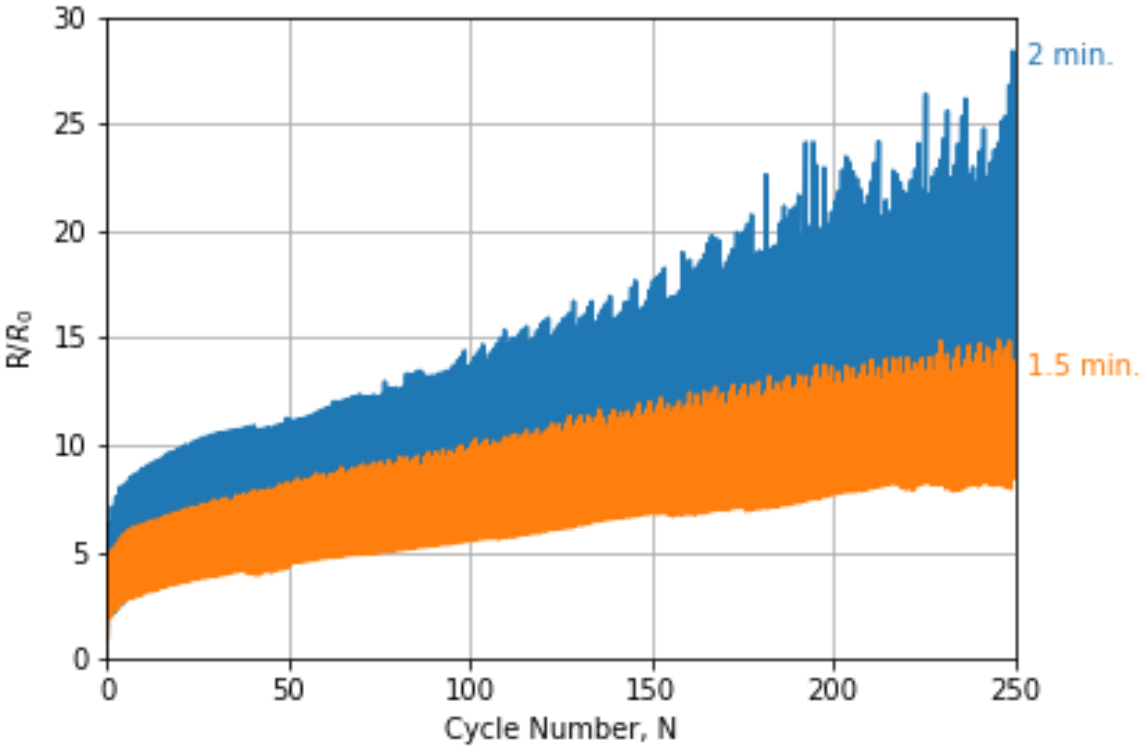

Figure 3-3: The flexibility results at 30% strain over 250 cycles of 1:6 A30UL AgNW:AgMf hybrid ECAs ultrasonicated for 10 minutes, then vortex mixed for 90 seconds and 120 seconds.

3.3 Nanowire:Microflake Ratio

The ratio of the AgNWs to AgMfs is important in determining the properties of the ECA. AgNW/AgMf ECAs were prepared at different ratios using both A30UL (30 nm diameter, 150 µm length, 10 mg/mL in ethanol) and B45 (45 nm diameter, 10 µm length, wet powder) AgNWs and analyzed. Long, thin AgNWs and shorter, thicker ones were chosen as long, thin AgNWs tend to agglomerate more readily than shorter, thicker ones due to their larger surface-area-to-volume ratios [78]. The conductivity results are shown in Figure 3-4. The ECAs with a 0% AgNW fill are pure AgMf ECAs. These results reflect similar trends seen in literature [71]: the resistivity of the ECA improves with the addition of nanowires at lower NW:Mf ratios, but gets worse at higher ratios. The most conductive samples are the 1:4 and 1:5 for the B45 and A30UL AgNWs, respectively. As expected, the optimal ratio of the A30UL AgNWs is lower than the optimal ratio of the B45 AgNWs due to increased agglomeration of longer, thinner nanowires.

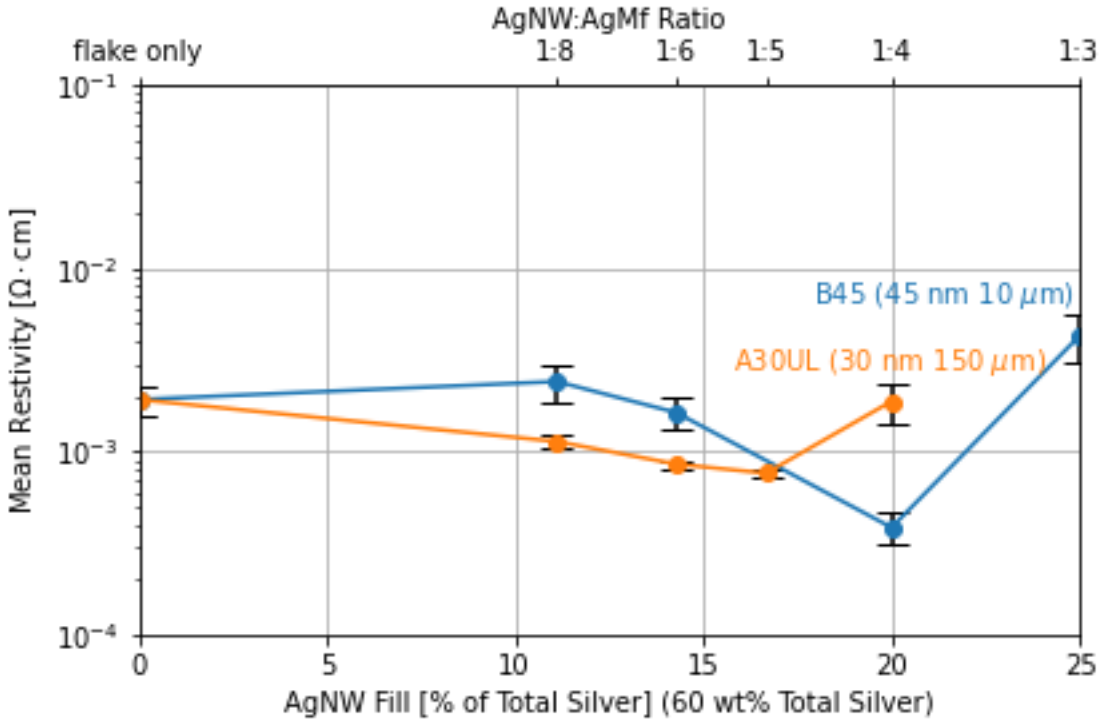

Figure 3-4: The conductivity of the hybrid ECA as a function of the AgNW to AgMf ratio at 60 wt% total silver. The 0% AgNW fill represents a pure AgMf ECA.

SEM images of the A30UL samples, shown in Figure 3-5, confirm the expected behaviour of the AgNWs. As the AgNW fill increases, from 1:8 to 1:5, and more AgMfs are replaced by AgNWs (as the total silver fill is kept constant), the conductivity improves as more AgNWs are present to bridge neighbouring AgMfs. However, as the AgNW fill keeps increasing, past 1:5 to 1:4, the AgNWs begin agglomerating on the surface of the AgMfs, seen in Figure 3-5c). Thus, the additional NWs added are less effective at providing conductive pathways, while at the same time there are less flakes. Overall, then, there are fewer pathways which in turn lowers the overall conductivity of the ECA.

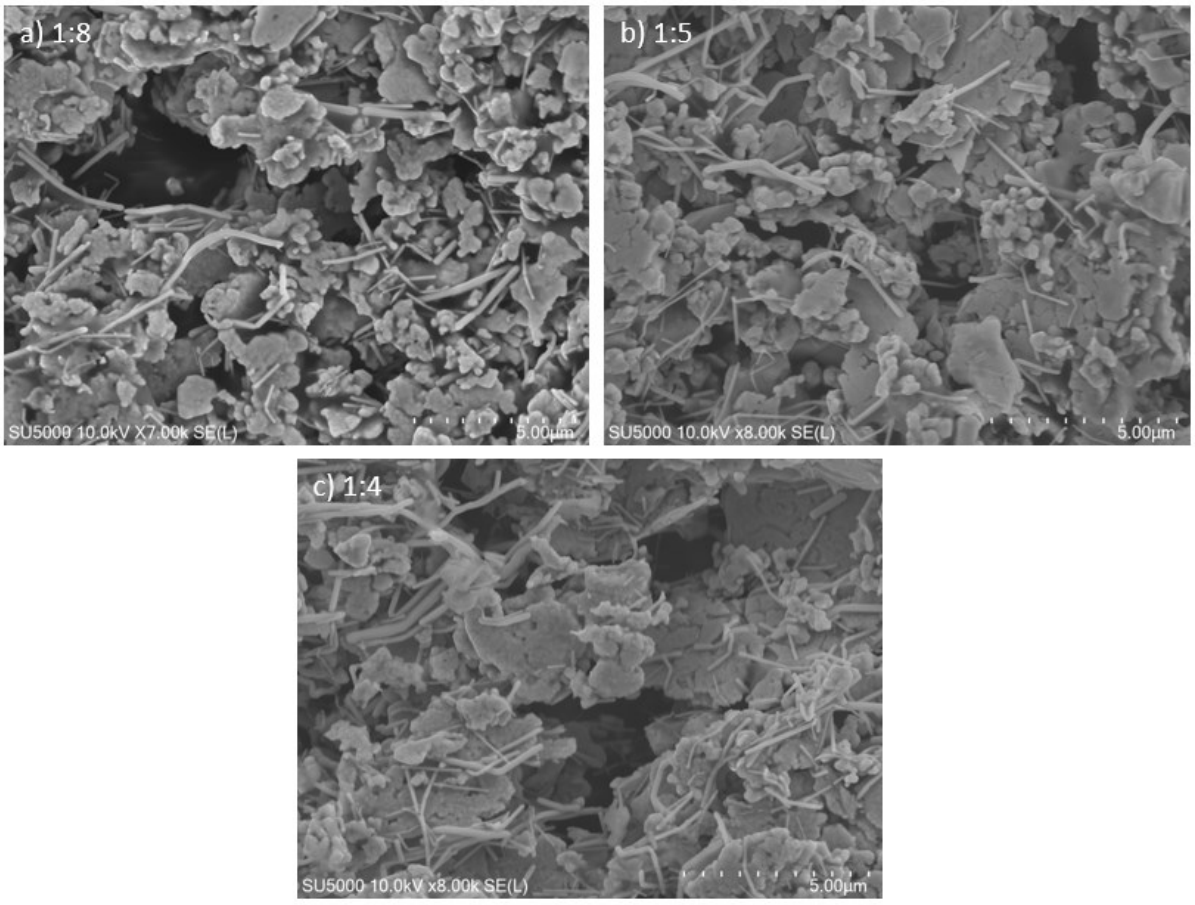

Figure 3-5: SEM images of A30UL AgNW/AgMf hybrid ECA samples prepared using ratios of a) 1:8 b) 1:5 and c) 1:4 AgNWs to AgMfs. The total silver fill fraction was kept constant.

The effect of the ratio on flexibility has not been studied before. The flexibility results of the various ratios are shown in Figure 3-6. The results align with the conductivity results: the B45 1:4 samples (20% AgNW fill) which are the most conductive, at approximately 3.9 x 10^{-4} Ω·cm, are also the most flexible with the resistance increasing 25x during the 100th cycle and recovering to 15x during relaxation. For A30UL, the 1:5 samples are the most conductive, at approximately 7.6 x 10^{-4} Ω·cm, and the most flexible with a resistance increase of 18x during the 100th cycle and recovering to 7x during relaxation. The flexibility results follow the conductivity trend for similar reasons. As the AgNW fill increases, more AgMfs are replaced by AgNWs. The flexibility improves since the NWs have a further reach than flakes and can thus better keep the network in contact when strained. At higher NW concentrations where they agglomerate (Figure 3-5c), they are less able to keep the network connected, especially with the lower flake density, which in turn decreases the flexibility.

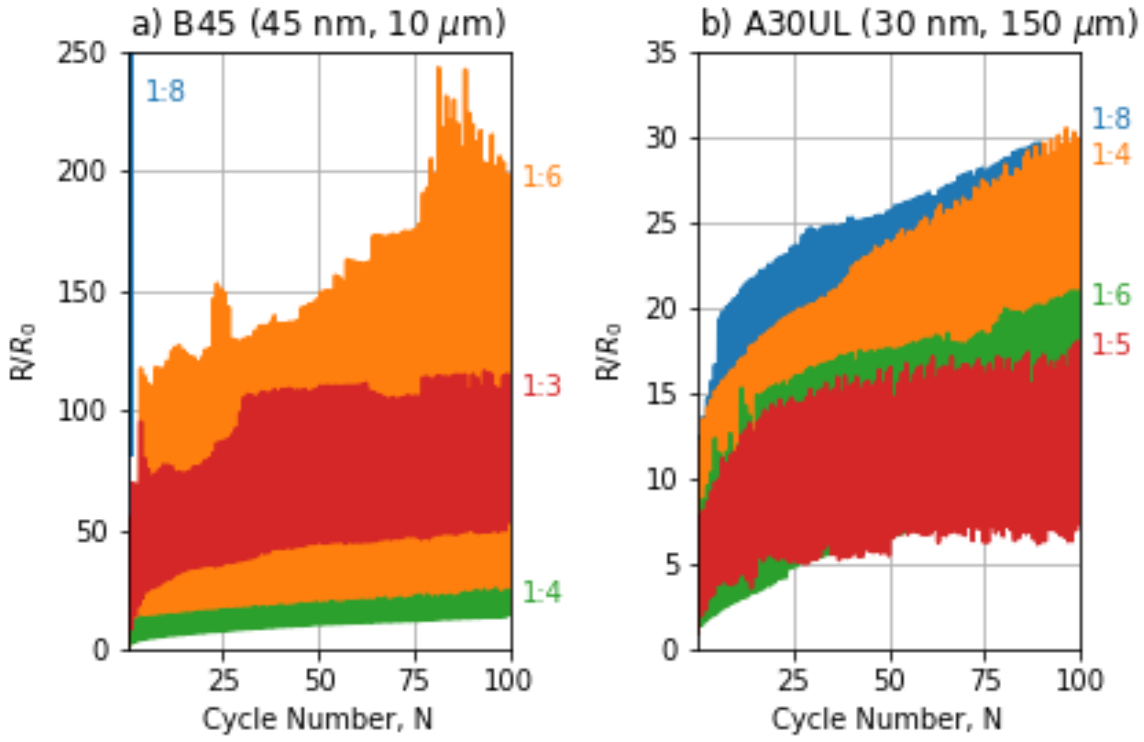

Figure 3-6: The flexibility results at 30% strain over 100 cycles of different ratios of a) B45 and b) A30UL AgNWs to AgMfs, at 60 wt% total silver. The 1:8 B45 ECA broke after the first cycle.

Due to the consistency of the results, i.e., better conductivity, and better flexibility, 1:4 and 1:5 were chosen as the optimal ratios for the B45 and A30UL AgNWs/AgMf ECAs, respectively.

3.4 Silver Nanowire Parameters

In addition to the processing parameters, the morphology of the AgNWs themselves, i.e., diameter and length, are important for determining the properties of the ECA and has not been studied before.

3.4.1 Length

To understand the impact of the length of the AgNWs on the properties of the ECA, 1:6 AgNW/AgMf hybrid ECAs were prepared with AgNWs with an average diameter of 30 nm and lengths of 5, 30 and 150 µm (A30SL, A30 and A30UL). The total weight of NWs was kept the same, which means that there are a fewer number of NWs in the samples using longer NWs compared to samples using short NWs. The conductivity results (Figure 3-7a) clearly show that as the length of the AgNWs increase, the resistivity decreases. The formulation with 150 µm long NWs had a mean resistivity of 8.6 x 10^{-4}

Ω·cm. SEM imaging, shown in Figure 3-8, helps further explain the trend. It can be seen that the longer NWs (Figure 3-8b) traverse the gap between flakes much better, and thus better keep the network in electrical contact. The shorter NWs on the other hand appear to settle in the gaps between the AgMfs instead of bridging them. Furthermore, electrons must traverse more particle-particle junctions when moving through shorter NWs, and these contacts are higher resistance than the NWs and flakes themselves.

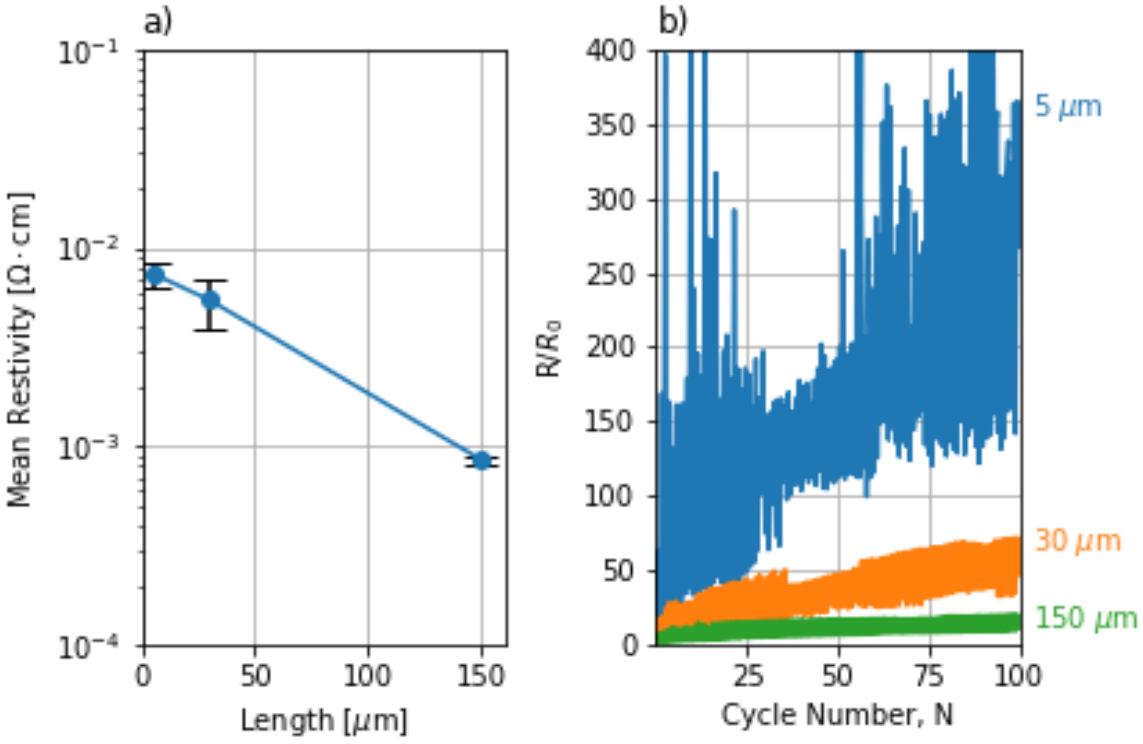

Figure 3-7: The a) resistivity and b) flexibility dependence on the length of 30 nm diameter AgNWs in 1:6 AgNW/AgMf hybrid ECAs.

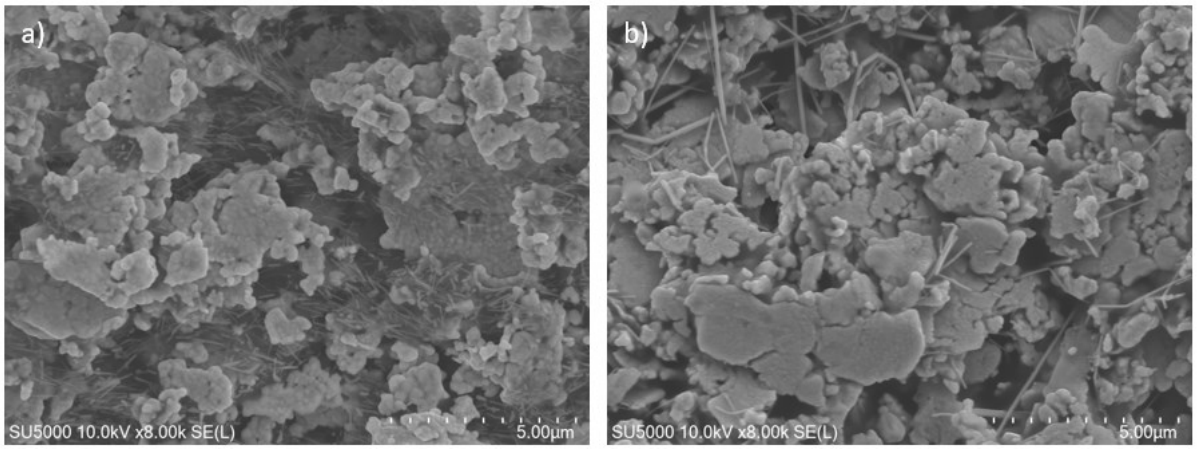

Figure 3-8: SEM images of 1:6 30 nm diameter AgNW/AgMf hybrids ECAs with lengths of a) 5 µm and b) 150 µm.

The flexibility results are shown in Figure 3-7b). As expected, the ECAs with longer nanowires better retain their resistance with straining. When strain is applied to the system, the AgNWs can deform and rotate to accommodate the applied stress [61]. The longer nanowires provide a longer reach which helps keep the network in better electrical contact. The resistance of the 1:6 A30UL ECA sample increased 21x during the 100th cycle and recovered to 11x during relaxation.

The results of the single-lap shear tests are shown in Figure 3-9. For this set of tests, only the A30 (30 µm) and A30UL (150 µm) AgNWs were used and two samples of each were prepared. One of the A30UL AgNW ECAs broke after curing indicating a low bonding strength. The tests indicate that ECAs prepared with shorter AgNWs have higher shear strengths than samples prepared with longer AgNWs. Both the A30 and A30UL samples failed adhesively (adhesive delaminated from the substrate) and cohesively (adhesive ripped apart). Furthermore, from an experimental perspective, I found it was more difficult to remove excess ethanol from the longer AgNW solutions while decanting. The residual ethanol that could not be removed made the longer AgNW ECAs more difficult to print on the aluminum and they did not hold their shape as well. This issue was not seen with the flexibility samples due to a strong adhesion to the TPU substrate.

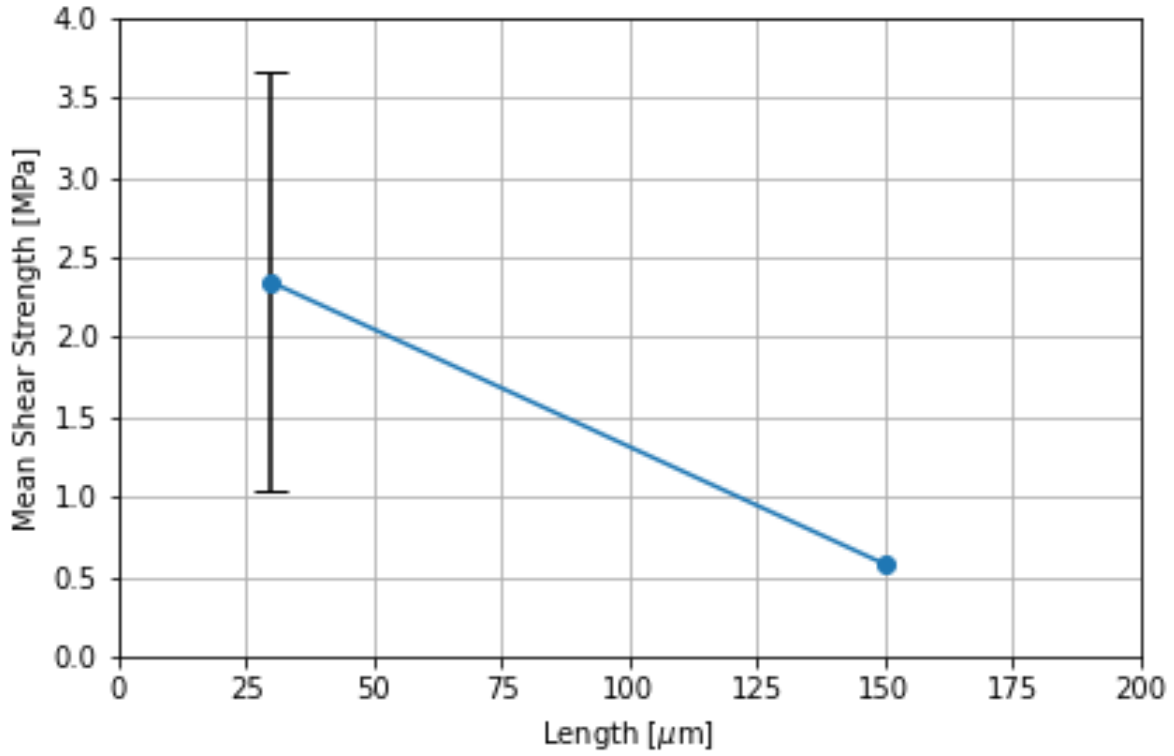

Figure 3-9: The single-lap shear test results of 1:6 30 nm diameter AgNW/AgMf hybrid ECAs with two different AgNW lengths.

Despite showing poor adhesion results, the longer 150 µm AgNWs were selected as the optimal length for the AgNW/AgMf hybrid ECA due to their superior conductivity and flexibility results. As will be demonstrated in subsequent chapters, the lower adhesion strength is still sufficient for real world applications as the ECA is able to bond a through-hole LED onto a TPU substrate (Chapter 4).

3.4.2 Diameter

The effect of the diameter on the properties of the ECA was studied by preparing 1:5 AgNW/AgMf hybrid ECAs using 150 µm long nanowires with diameters of 30, 70 and 100 nm (A30UL, A70UL and A100UL). The conductivity results are shown in Figure 3-10a). The three diameters of AgNWs show approximately the same conductivity, on the order of 2 - 3 x 10^{-3} Ω·cm. There are multiple factors that appear to negate each other. On one hand, thinner nanowires sinter better at lower temperatures. The 150 °C used in the fabrication procedure has been shown to be the optimal sintering temperature for these same 30 nm AgNWs which leads to the highest network conductivity [76]. The optimal sintering temperature of the thicker nanowires is higher. On the other hand, the constriction resistance at the

nanowire junctions is higher for thinner nanowires because of the smaller area of the contact. Furthermore, the conductivity of the thinner nanowires themselves is lower than that of thicker nanowires [79] since the electrons are closer to the surface where they can scatter. Lastly, thinner AgNWs are more susceptible to damage and breaking from the mixing procedures, which was shown in Section 3.2.1 to lower network conductivity.

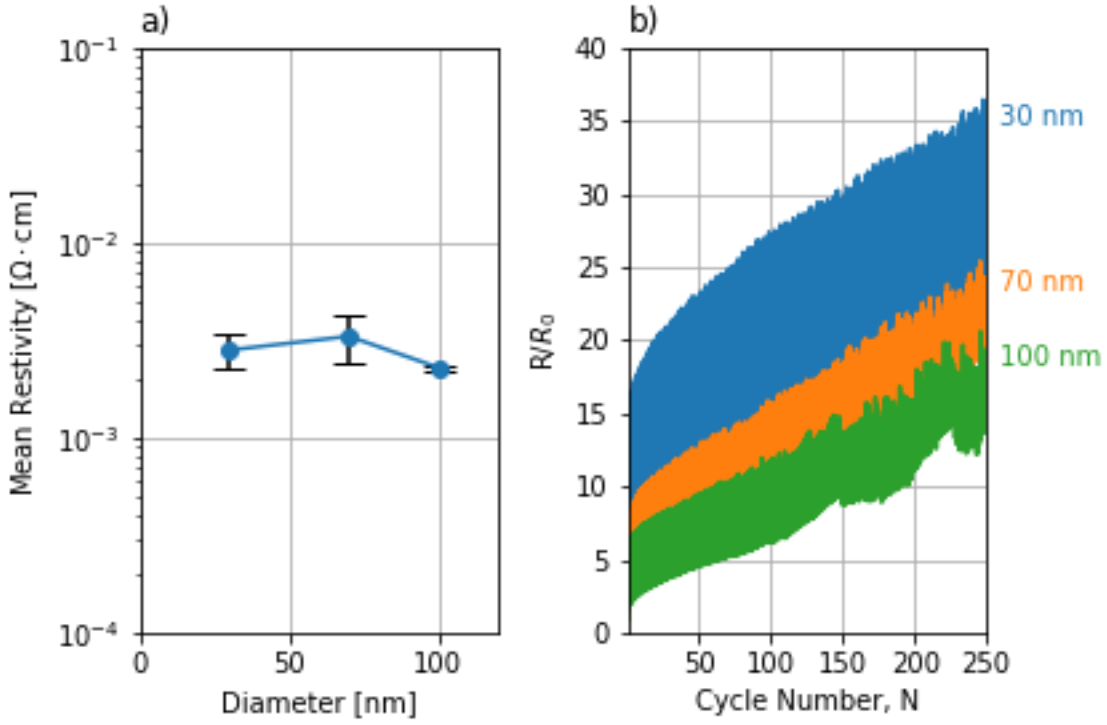

Figure 3-10: The a) conductivity and b) flexibility dependence on the diameter of the AgNWs for 1:5 150 µm long AgNW/AgMf hybrid ECAs.

The flexibility results are shown in Figure 3-10b). There is a clear trend that samples with thicker nanowires are more flexible. During the 250th cycle of 30% strain, the resistance increased 36x, 24x and 19x for the 30 nm, 70 nm, and 100 nm AgNW samples, respectively. During relaxation, the resistance recovered to 21x, 21x and 16x, respectively, and after 10 minutes of relaxation, the samples recovered to 11x, 7.9x and 4.8x, respectively. SEM images of samples containing 30 nm and 100 nm diameter NWs after strain cycling are shown in Figure 3-11. Compared to a similar sample before strain was applied (Figure 3-5b), the 30 nm diameter NWs in Figure 3-11a) appear more bunched up while the 100 nm diameter NWs in Figure 3-11b) remain better dispersed. This is likely due, in part, to the fact that there are a higher number of NWs when thinner NWs are used and they have larger surface-area-to-volume ratios, which causes more agglomeration when they are brought closer together during

straining. Also, one would expect thinner NWs to break more easily with stretching, and indeed it appears that the average NW length is less in the thinner NW sample after straining. The thinner NWs also incur more damage during the mixing procedures which could make them more susceptible to breaking under applied stress.

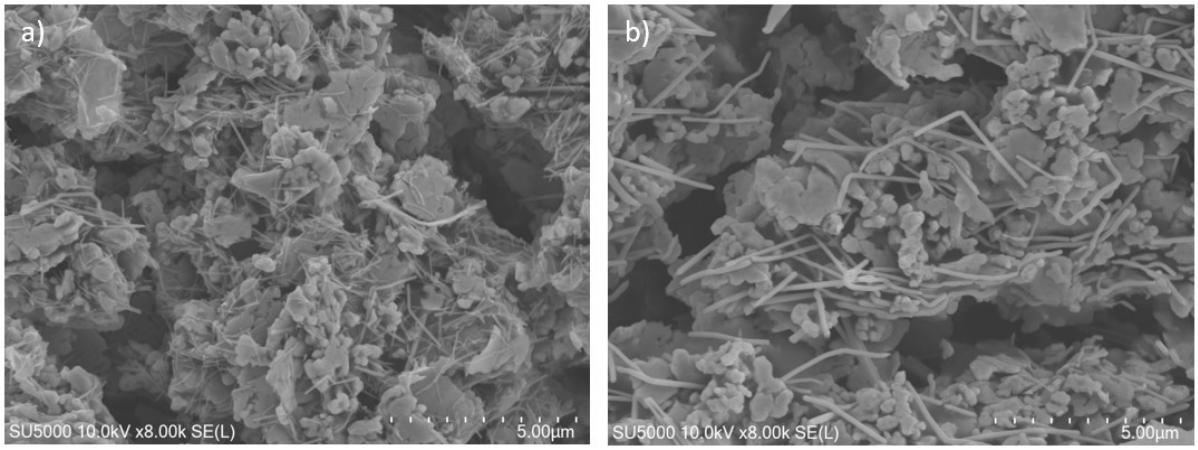

Figure 3-11: SEM images of 1:5 150 µm long AgNW/AgMf hybrids ECAs after strain cycling with diameters of a) 30 nm and b) 100 nm.

For the single-lap shear tests, test coupons were prepared using 1:6 AgNW/AgMf hybrids ECAs with A30 (30 nm, 30 µm), A50 (50 nm, 40 µm), B45 (45 nm, 10 µm), and B100 (100 nm, 10 µm) AgNWs. The A30 and A50 AgNWs are solution based at 10 mg/mL in ethanol and the B45 and B100 are wet powders. Two coupons of each size AgNW were prepared. The results are shown in Figure 3-12. For the wet powder AgNWs, the larger diameter has a larger shear strength at the same AgNW length. For the solution based AgNWs, the larger diameter also has a larger shear strength, even at a slightly longer AgNW length which, as shown in Section 3.4.1, should negatively impact the shear strength of the formulation. Thinner nanowires have a higher surface-area-to-volume ratio. This leads to a higher total amount of NW surface area in the sample, and as discussed in a paper where carbon nanotubes were used in an ECA [80], more of the epoxy resin is thus attracted to NW surfaces and away from the adherend (substrate) [80].

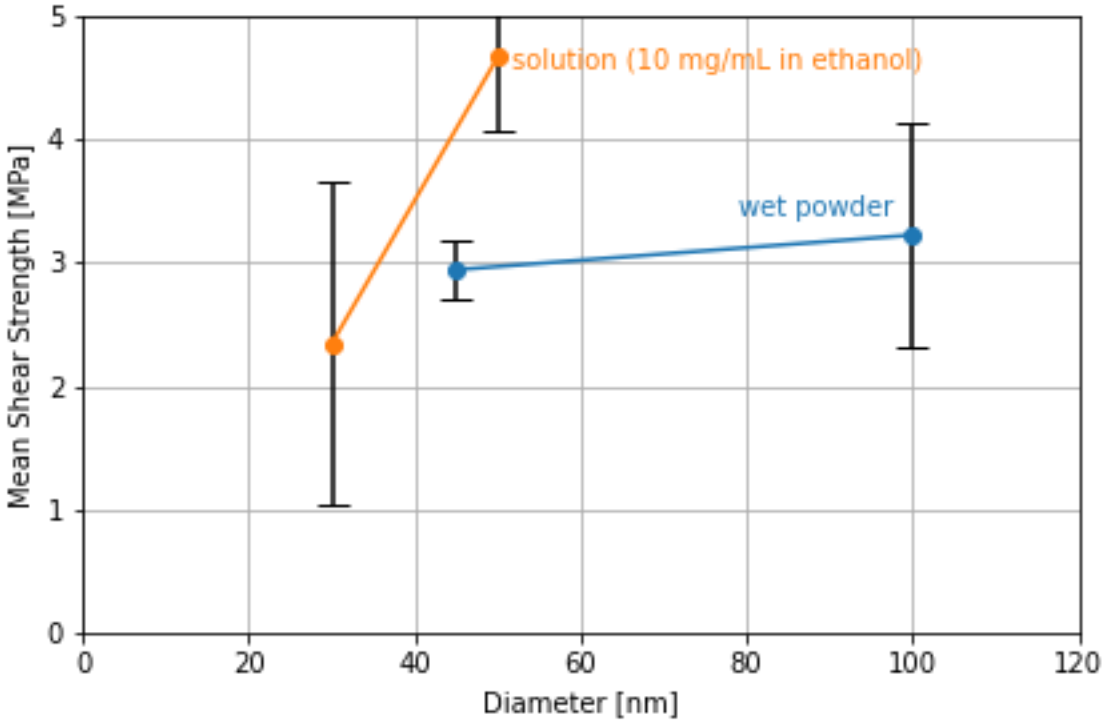

Figure 3-12: The single-lap shear test results for 1:6 AgNW/AgMf hybrid ECAs prepared with different diameter AgNWs. The solution based A30 and A50 AgNWs have lengths of 30 and 40 µm, respectively, while the wet powder B45 and B100 both have lengths of 10 µm.

Based on these results, i.e., the improved mechanical properties without sacrificing electrical properties, the larger diameter AgNWs were selected as optimal for improving the properties of ECAs.

3.5 Baseline Comparison

By narrowing in on the fabrication steps relevant to nanowires and studying the effect of the nanowire dimensions on the properties of the ECA, ECAs with improved conductivity and flexibility compared to flake-only ECAs were achieved. The results are shown in Figure 3-13 and Figure 3-14. Using the A30UL (30 nm diameter, 150 µm length, 10 mg/mL in ethanol) and B45 (45 nm diameter, 10 µm length, wet powder) NWs, resistivities as low as 7.6 x 10^{-4} Ω·cm and 3.9 x 10^{-4} Ω·cm, respectively, were achieved compared to 1.9 x 10^{-3} Ω·cm for the in-house fabricated flake-only ECA. After 100 cycles to 30% strain, resistance increases as low as 9.8x were demonstrated compared to 25x for the flake-only ECA. As shown in Figure 3-14b), the flake-only ECA lost conductivity after 75% strain while an A30UL AgNW/AgMf ECA was able to sustain conductivity at even 120% strain. The commercial ECA broke while being strained to 30%.

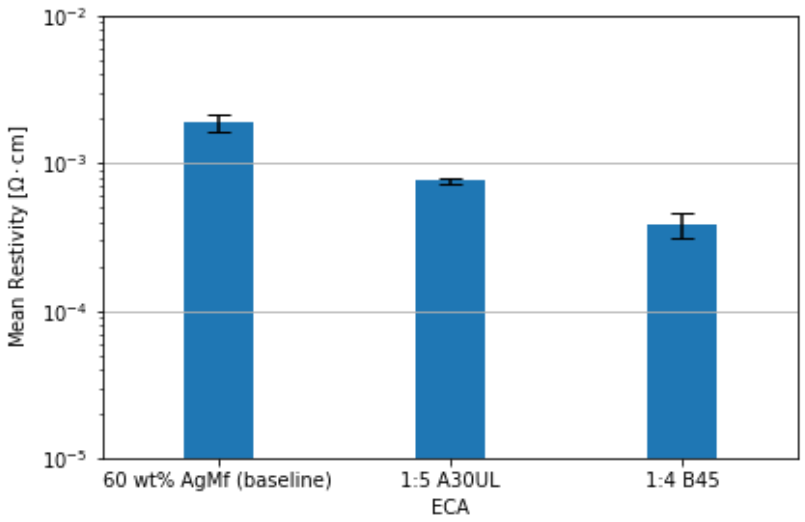

Figure 3-13: The improved conductivity of the AgNW/AgMf ECAs compared to the baseline flake-only ECA. All ECAs have a total silver content of 60 wt%.

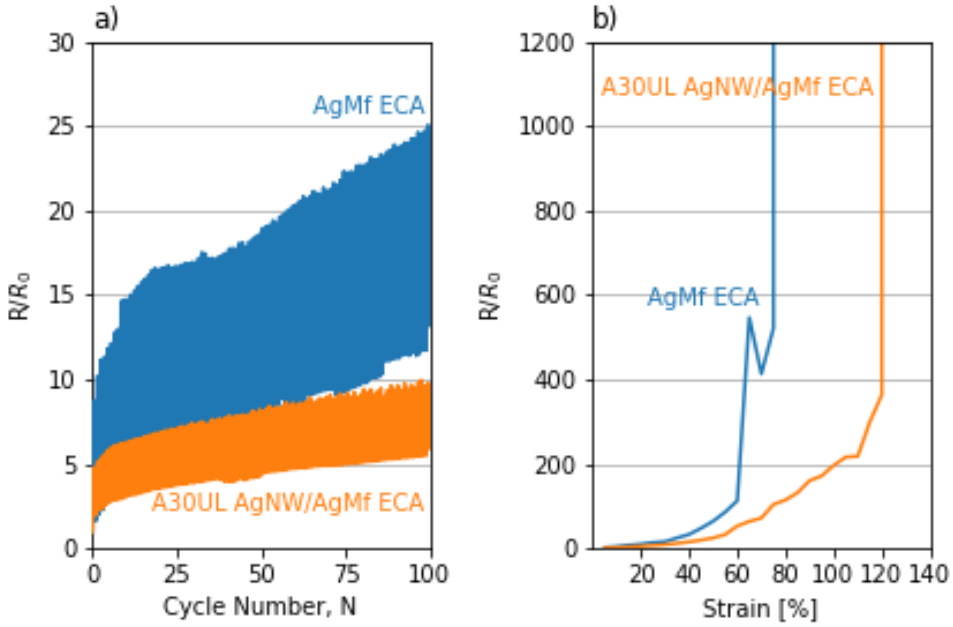

Figure 3-14: The a) strain cycling to 30% and b) maximum elongation results of the AgNW/AgMf ECAs compared to the baseline flake-only ECAs.

Shorter and thicker nanowires demonstrated better shear strengths than longer and thinner nanowires but the shear strength of all the hybrid AgNW/AgMf ECAs was lower than the baseline AgMf ECAs. The results are shown in Figure 3-15. Using the larger diameter NWs, which also showed a superior flexibility, should alleviate some of the shear strength concerns with using the longer NWs.

Furthermore, as will be demonstrated in Chapter 4, the shear strength of a hybrid ECA using the optimized parameters is sufficient for real-world applications. However, if a higher shear strength is required, methods not explored in this chapter, such as a lower metal fill (lower than the 60 wt% used here) or using a solvent-free formulation [37], could be explored. NW networks have a far lower percolation threshold than networks of flakes. And further, hybrid ECAs have an even lower percolation threshold than either of the structures individually due to the synergistic effect of the two fillers [64]. This allows the use of lower fill fractions. While the conductivity would be slightly reduced, the shear strength should increase due to more epoxy resin present. Since, as demonstrated in this chapter, the hybrid AgNW/AgMf ECAs have a higher conductivity than the flake-only ECA, the slight decrease in conductivity should not be a concern.

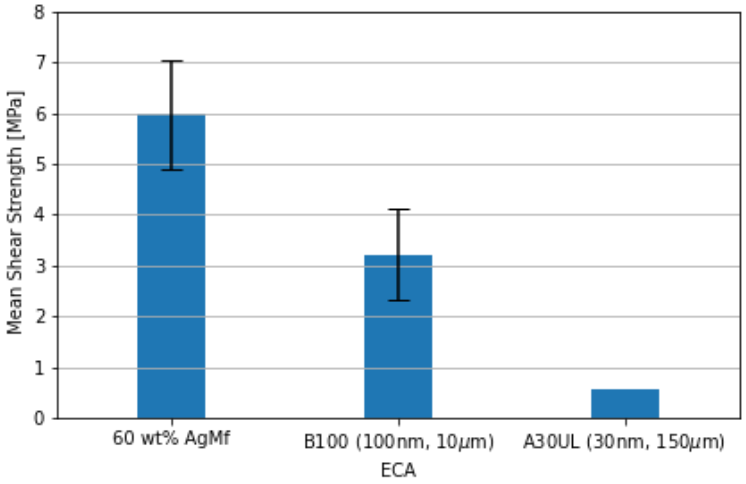

Figure 3-15: The shear strength of the AgNW/AgMf ECAs compared to the baseline flake-only ECA.

3.6 Conclusion

In this chapter, the fabrication procedure for AgNW/AgMf hybrid ECAs was presented. Key parameters in the procedure, namely the ultrasonication time, vortex mixing time and the AgNW to AgMf ratio, were studied and optimized. The optimal parameters found are given in Table 3-2. The influence of the diameter and length of the nanowires on the properties of the ECA were also investigated. Longer nanowires demonstrated superior conductivity and flexibility, compared to shorter nanowires, but a lower shear strength. The diameter of the AgNWs did not affect the electrical properties of the ECA, but larger diameters improved the mechanical properties, both flexibility and adhesion strength. Therefore, longer, thicker nanowires are chosen for the optimal ECA formulation and will be used in the demonstration device presented in the next chapter.

Table 3-2: Optimized parameters for the fabrication of highly conductive, flexible AgNW/AgMf hybrid ECAs.

Parameter	Optimal Value
Ultrasonication Time	5 - 10 min. *dependent on further flexibility results
Vortex Mixing (post hardener)	1.5 min.
AgNW to AgMf Ratio	1:5 for A30UL AgNWs 1:4 for B45 AgNWs
Length	150 µm (UL series)
Diameter	100 nm

Chapter 4
Demonstration Device

In the previous chapter, the electrical and mechanical performance advantages of the nanowire/microflake ECAs over pure microflake ECAs were demonstrated through in-lab characterization. In this chapter, the real-world viability of the ECAs for flexible hybrid electronics is demonstrated through the preparation and characterization of a light emitting diode (LED) integrated onto a flexible substrate (TPU). The LED, through changes in its intensity, provides real-world, observable feedback to changes in the ECA as the device is strained. After the real-world validation of the ECA, the LED device is used to create a wearable, flexible LED patch.

4.1 Device Setup

4.1.1 Fabrication

To prepare the devices, strips of the ECA were prepared in the same manner as for the flexibility tests described in Section 2.2.3. Before the precure step, the LED was mounted onto the TPU substrate via the ECA. The leads of the LED were bent to allow a good connection with the ECA and pressure was applied with a binder clip during curing to embed the LED in the ECA to establish a strong mechanical connection. Two pieces of aluminum, covered with Teflon to prevent them from sticking to the ECA/substrate, were placed inside the binder clip to distribute pressure more evenly across a larger area. Fabricated devices after curing, with and without the binder clip, are shown in Figure 4-1. Two parallel strips of ECA, as opposed to creating a gap in one strip, were used to ensure uniform strain was applied to the ECA. The devices were cured in the vacuum oven, as opposed to the hot plate, as the devices could not make good contact with hot plate surface due to the binder clip.

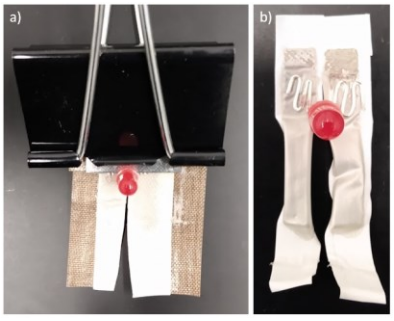

Figure 4-1: a) A flexible device post curing. The binder clip is used to apply pressure to the LED leads during curing. b) A flexible device ready for testing (with the tools used for curing removed).

4.1.2 Testing Methodology

The testing methodology is based on a similar printed, flexible device [81]. A modified version of the flexibility tests described in Section 2.2.3 was employed to test the devices. The LED end of the sample was placed in the stationary clamp, and the end opposite of the device was clamped to the moving linear stage. While the LED end of the sample was placed in the stationary clamp, the LED itself was not supported by the clamp and only held in place by the ECA. The test setup was placed in a closed cardboard box to block out ambient light, which would interfere with measurements of the LED intensity. A piece of insulating tape was stuck onto the metal portions of the linear stage clamps to prevent them from creating a short circuit. An external DC power supply (GQ-A305D, GQ Electronics LLC) set at 5 V applied power to the device during testing. A cellphone on the cardboard box took photos of the device through a small, 2 cm x 2 cm, opening in the box.

The tests were run using a modified version of the software described in Section 2.2.3.1. The strain cycling was unchanged, except instead of taking resistivity measurements during straining/relaxation, the software would issue commands via the Android Debug Bridge to the connected cellphone to take photos of the device.

4.1.3 Data Analysis

To extract intensity information from the photos, a separate program was written using the Python™ programming language. The program would read the images in as grayscale and crop them to the relevant portion containing the LED. Based on the position of the LED in the image, it would select a column of pixels and compare their values to the maximum intensity of the LED. The steps are shown in Figure 4-2. Image manipulation, such as cropping, and analysis were performed using the OpenCV library.

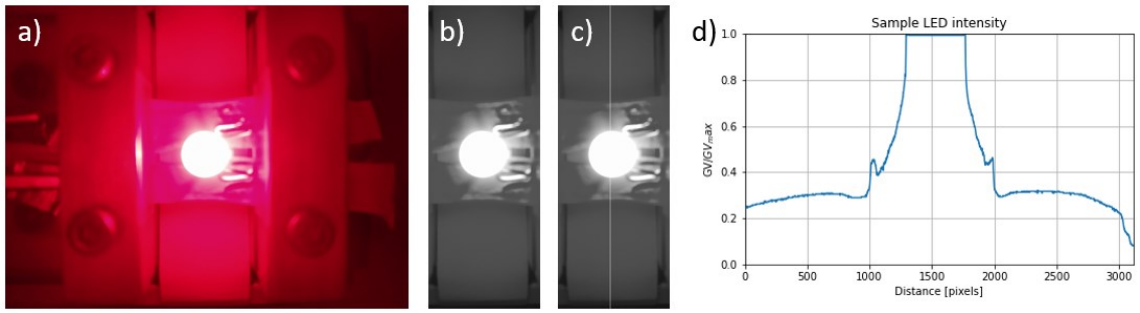

Figure 4-2: The processing steps to extract the intensity data from images of the device: a) the original image, b) the cropped grayscale image, c) a column of pixels is selected, shown in white, and d) the intensity

plot from the selected column. Features in the image, such as the light reflecting off the ECA strips, are visible in the plot.

4.2 Characterization

To characterize the fabricated devices, the devices were strain cycled at 20%. 20% strain was chosen for the demonstration as this is the maximum strain typically seen in wearable applications [82].

4.2.1 Baseline Results

The results of strain cycling the LED device using the flake-only ECA at 20% strain for 300 cycles are shown in Figure 4-3. The slight decrease in the intensity of the LED from the initial state to subsequent states is due to the LED shifting (tilting) after the initial strain cycle. The LED turned off while under strain after 217 cycles but recovered during relaxation. After 256 cycles, the LED did not turn back on during relaxation. This is consistent with one of the main issues of conventional ECAs – poor flexibility.

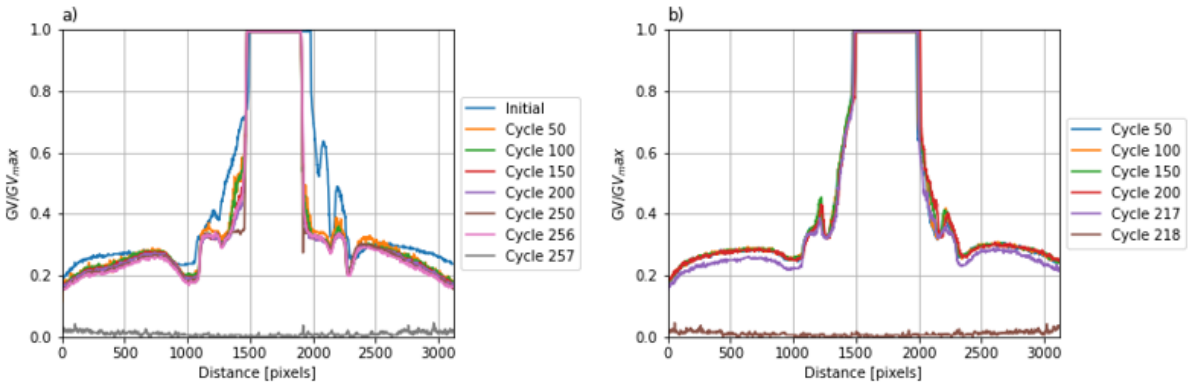

Figure 4-3: The measured intensity of the LED using the flake-only ECA during a) relaxation and b) straining at various cycles during strain cycling at 20% for 300 cycles.

An inspection of the device after the strain cycling was completed revealed tears in the ECA strips and TPU substrate at approximately the halfway point between clamps, as shown in Figure 4-4a). This same failure mode occurred in other flake-only devices prepared as shown in Figure 4-4b). In addition to the stress applied by the linear stage, the ECA/substrate has to now support the load of the LED too. It is believed this, and the weight of the LED tilting during straining/relaxation, contribute to the tear. Unlike the commercially available ECA from Chapter 2, where only the ECA ruptured during straining, the ECA and substrate were both torn in this case indicating a strong bond between ECA and substrate. It is known that the tearing is not a result of the pressure applied during curing as the torn portion was not under pressure during curing.

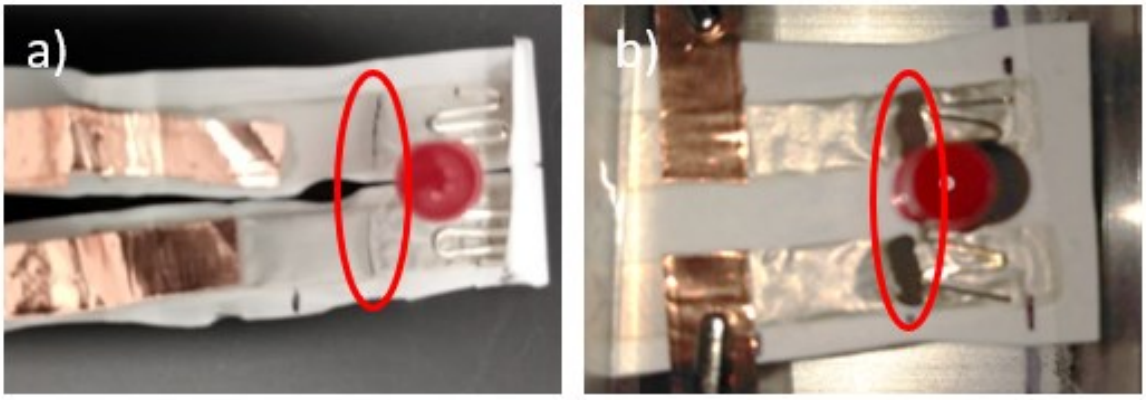

Figure 4-4: a) The baseline device after 300 cycles to 20% strain. The tears in the devices are circled in red. b) An earlier flake-only prototype exhibiting the same mode of failure.

4.2.2 Optimized ECA

The results of strain cycling the LED device using the optimized hybrid nanowire/microflake ECA (1:5 A100UL, prepared using 10 minutes of ultrasonication) at 20% strain for 500 cycles are shown in Figure 4-5. The device did not show any decrease in intensity during any of the cycles reflecting the excellent mechanical and electrical properties of the optimized ECA and the ability of the ECA to maintain these properties. The slight decrease in the intensity of the LED from the initial state to subsequent states during relaxation is due to the LED shifting (tilting) after the first strain cycle as shown in Figure 4-6. During the first strain cycle, the weight of the LED shifted, and it remained in that position for subsequent measurements. However, this did not impact the electrical or mechanical connection between the LED and ECA as shown by the unchanging intensity during straining in Figure 4-5b).

The ability of the ECA to resist tearing and breaking during repeated straining is a result of the increased cohesive strength of the nanowire-containing ECA compared to the flake-only ECA. The larger total surface area of the nanowires compared to flakes allows them to absorb more of the epoxy resin onto them. This lowers the adhesion strength of the ECA as seen in Chapter 3, but increases the ECA's cohesive strength and therefore, ability to withstand tearing and ripping during repeated straining [80].

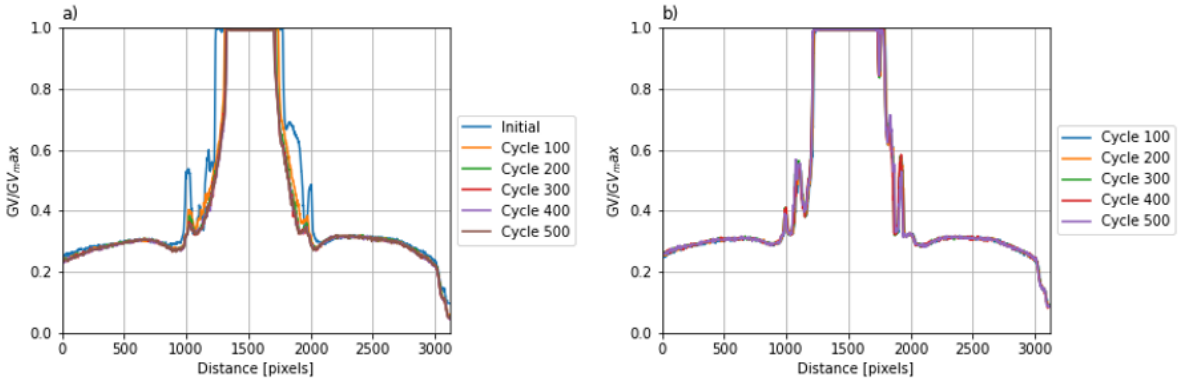

Figure 4-5: The measured intensity of the LED using the optimized nanowire/microflake ECA during a) relaxation and b) straining at various cycles during strain cycling at 20% for 500 cycles.

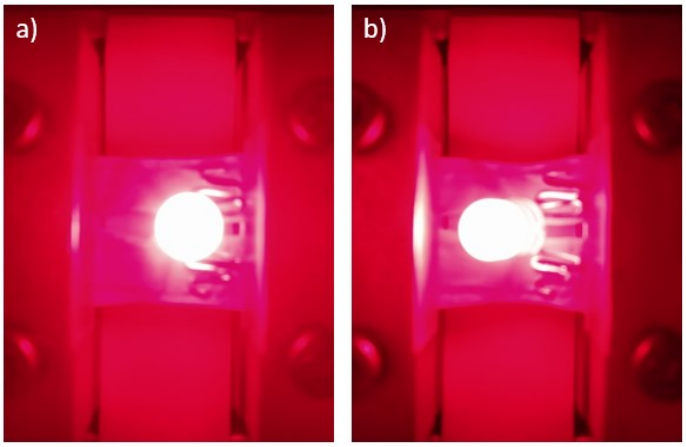

Figure 4-6: The LED attached to TPU using the optimized ECA a) before and b) after 500 cycles at 20% strain. During the first strain cycle, the position of the LED shifted but the ECA maintained an excellent electrical and mechanical connection.

4.3 Flexible Hybrid Electronics

With the viability of the optimized ECA for real-world applications having been demonstrated, the LED device was used to fabricate a wearable, flexible LED patch using the steps from Chapter 1. The optimized ECA device was encapsulated using a second TPU layer and then laminated onto a stretchable fabric in an oven at 120 °C using the binder clip/aluminum method described earlier. The fabric could be any textile, such as athletic wear or a vehicle seat cover. The fabricated FHE device is shown in Figure 4-7. Laminating the device onto the textile at the end allows the separation of the technology layers from the textile layers. In an industrial setting, the garment/textile and technology layer could be manufactured separately, in different facilities, and then brought together at the end. A small portion of the ECA strips were left unencapsulated to allow a connection to an external power source.

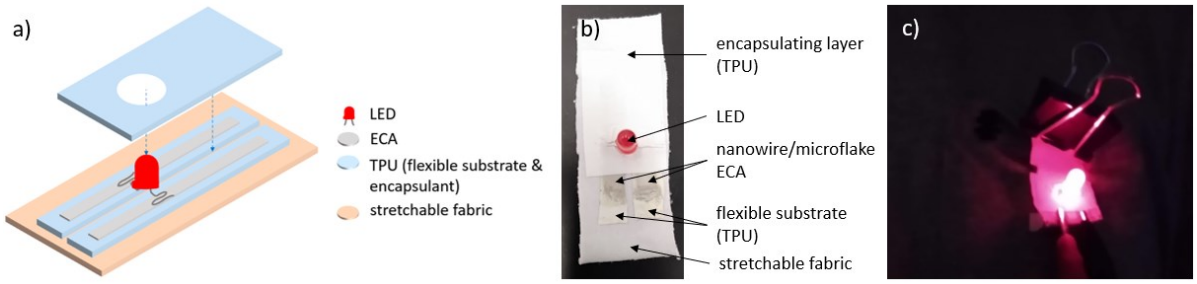

Figure 4-7: a) A schematic of the wearable, flexible patch. b) The wearable, flexible LED patch created from the optimized ECA device laminated onto a fabric and encapsulated with TPU. c) The LED patch clipped to a t-shirt.

4.4 Conclusion

In this chapter, the fabrication procedure and flexibility testing methodologies from previous chapters were adapted to print and test a real-world equivalent device – an LED on a flexible substrate. Through changes in the intensity of the LED, the device provided observable feedback on changes in the ECA and the connection between the ECA and LED during straining/ relaxing. In this case, the main change observed was the LED turning off after repeated strain cycling in the baseline device which used a flake-only ECA. The LED turned off while under 20% strain after 217 cycles but recovered during relaxation. After 256 cycles, the LED did not turn back on during relaxation. A device utilizing the optimized nanowire/flake ECA (1:5 A100UL prepared using 10 minutes of ultrasonication) showed no change in the intensity of the LED during strain cycling to 20% strain over 500 cycles demonstrating the excellent mechanical and electrical properties of the ECA as well as its durability. With the viability of the optimized ECA demonstrated, the LED device was used to create a wearable, flexible LED patch.

Chapter 5
Conclusions and Future Work

5.1 Conclusions

In this work, silver nanowire-enhanced microflake electrically conductive adhesives (ECAs) were formulated as a flexible, conductive interconnect for flexible hybrid electronics (FHEs). The nanowire/microflake ECAs showed improved conductivity and flexibility over conventional microflake ECAs. The nanowire/microflake ECAs showed resistivities as low as 3.9×10^{-4} Ω·cm, compared to 1.9×10^{-3} Ω·cm for the flake-only ECA. After 100 cycles to 30% strain, the resistance of the nanowire/microflake ECA only changed 9.8x while the resistance of the flake-only ECA changed by 25x. A commercially available ECA broke while being strained to 30%. Despite showing a lower shear strength, the real-world viability of the nanowire/microflake ECA was demonstrated through the integration of a light-emitting diode (LED) on a flexible substrate.

The improved properties of the nanowire/microflake ECA were achieved by focusing on the steps and parameters relevant to the nanowires and optimizing for them. In Chapter 2, the fabrication procedure for conventional ECAs was presented and the testing methodologies for the conductivity (four-point probe), flexibility (strain cycling using a linear stage) and shear strength (single-lap shear strength tests following the ASTM D1002 standard) of the ECA were established. The fabrication procedure and testing methodologies were used to prepare and characterize a flake-only ECA and a commercially available ECA to establish a baseline against which the nanowire/microflake ECA would be tested against.

In Chapter 3, silver nanowires were integrated into the microflake ECAs using different processing parameters and nanowire dimensions. The nanowires bridge neighbouring microflakes to improve the conductivity and the nanowire network can rotate and deform under strain to maintain an electrical connection. It was found that during the initial phases of ultrasonication, up to approximately 10 min., the sonication primarily works to disperse the conductive filler in the epoxy resin. Further ultrasonication, beyond 10 min., primarily functions to damage the nanowires, which degrades the properties of the ECA. Similar mechanisms were observed with prolonged vortex mixing. It was also shown that there is a fine-balance between the amount of nanowires and flakes in the ECA for a fixed total silver content. If an insufficient amount of nanowires are added, the ECA will underperform. If too many nanowires are added, they agglomerate on the surface of the flakes and degrade the properties of the ECA. Longer and thinner nanowires have a lower optimal ratio than shorter and thicker nanowires

as they are more prone to agglomeration. The A30UL nanowires (30 nm, 150 μm, 10 mg/mL in ethanol) had an optimal ratio of 1:5, while the B45 nanowires (45 nm, 10 μm, wet powder) had an optimal ratio of 1:4. ECA prepared with longer nanowires showed an improved conductivity and flexibility over an ECA prepared with shorter nanowires of the same diameter. Finally, it was found that the nanowire diameter does not impact the conductivity of the ECA but larger diameters showed better flexibility. Shorter and thicker nanowires showed better shear strengths than longer and thinner nanowires, but the shear strength of all the nanowire/microflake ECAs was lower than the conventional ECAs. However, it was demonstrated in Chapter 4 that the strength of even the ECAs containing long nanowires was sufficient for real-world applications.

In Chapter 4, an LED was integrated onto a flexible substrate using the flake-only ECA and the optimized hybrid ECA. Using the conventional, flake-only ECA, the device failed after 256 cycles to 20% strain. In contrast, the device using the hybrid ECA did not show any change after 500 cycles to 20% strain reflecting the improved electrical and mechanical properties of the ECA and the ability of the ECA to maintain those properties. The optimized ECA device was encapsulated with an additional layer of TPU and laminated onto a stretchable fabric to create a wearable, flexible LED patch.

The novel contributions of this work to the field of ECAs for FHEs lie in three places: the investigation of the flexibility of nanowire-enhanced microflake ECAs, the investigation of the effect of the nanowire morphology on the properties of the ECA and the study of the effect of the mixing method on the ECA. For the first time, the improved flexibility of hybrid nanowire/microflake ECAs was shown. As the focus of ECAs thus far has been as a solder replacement, the flexibility of the ECA has been neglected. As shown in this work, AgMfs are not the ideal conductive filler for flexible ECAs. The conductive backbone formed by the AgMfs needs to be supported by an auxiliary filler that can maintain an electrical connection under strain. AgNWs are the most promising candidate for this. Furthermore, this work emphasized the importance of examining the properties of the conductive filler used. It is not enough to synthesize/purchase a batch of AgNWs and add them to the ECA as is usually done. The AgNWs need to be the correct diameter, length, and in the correct portion to the AgMfs to optimize the properties of the ECA. Finally, this work illustrates the importance of catering the fabrication procedure towards the conductive filler(s) used. Ultrasonication is a popular mixing method for ECAs, but as demonstrated in this work, prolonged ultrasonication deteriorates the properties of the ECA by damaging the silver nanowires.

5.2 Future Work

While sufficient progress has been made in this work to improve the electrical and mechanical properties of hybrid nanowire/microflake ECAs, there is more that needs to be understood and studied before they are ready for commercialization. One of the main issues that silver nanowire-based materials face is the oxidization and degradation of the nanowires over time, which in turn degrades the properties of the materials [78]. As only a small amount of nanowires are added to the microflake ECA and the nanowires are encapsulated in the epoxy resin, it needs to be investigated whether the nanowire degradation is a point of concern in this application and if it is, passivation techniques of the nanowires need to be explored.

Some next-generation substrates in the field of flexible hybrid electronics, such as textiles and paper, have lower temperature tolerances than the substrates used in this work and cannot tolerate curing temperatures of 150 °C. One of the advantages of silver nanowires over microflakes is their lower sintering temperature [33], [83]. As such, the viability of nanowire/microflake ECAs at lower curing temperatures should be investigated.

An additional advantage of silver nanowires that should be explored is their lower percolation threshold. Not only do silver nanowire networks have lower percolation thresholds than networks of flakes, ECAs using hybrid fillers have previously been demonstrated to have lower percolation thresholds than ECAs using either filler individually [64]. Using a lower metal fill could reduce the weight and cost of the ECA. Though this would reduce conductivity slightly, it is shown in this work that NWs improve the conductivity compared to flake-only ECAs so, depending on how much the metal fill is reduced, the conductivity could be maintained at a similar level to conventional 60 wt% flake-only ECAs while the mechanical flexibility should increase.

A potential limitation of the nanowire/microflake ECAs presented in this work is their lower shear strength compared to the flake-only ECA and commercially available ECA. If a higher shear strength is required, the use of metal fills less than the 60 wt% used in this work, as described in the previous paragraph, would improve the shear strength. It is recommended to also address the presence of residual ethanol after centrifuging, which has been identified in this work as a possible source of the lower shear strength. The optimization of the amount of ethanol added during the preparation of the nanowire/microflake ECAs should be investigated. The transition to a solvent-free formulation should also be considered as this has been shown to improve the shear strength of other hybrid ECAs [37]. To accomplish a solvent-free formulation, other mixing techniques will need to be explored.

Finally, the conductivity and flexibility of the ECAs using the optimal nanowires (100 nm diameter, 150 μm long) could be further refined and optimized. The ultrasonication, vortex mixing, and ratio optimization studies were performed using 30 nm diameter, 150 μm long nanowires as it is believed the longer and thinner nanowires are more susceptible to damage during mixing and more likely to agglomerate in the ratio optimization study. By replicating the studies with the 100 nm diameter, 150 μm long nanowires, incremental improvements in the properties of the optimized ECAs should be possible.

Letters of Copyright Permission

ELSEVIER LICENSE
TERMS AND CONDITIONS

Sep 20, 2021

This Agreement between Mr. Hubert Argasinski ("You") and Elsevier ("Elsevier") consists of your license details and the terms and conditions provided by Elsevier and Copyright Clearance Center.

License Number	5153240186655
License date	Sep 20, 2021
Licensed Content Publisher	Elsevier
Licensed Content Publication	Journal of Non-Crystalline Solids
Licensed Content Title	Low filled conductive P(VDF-TrFE) composites: Influence of silver particles aspect ratio on percolation threshold from spheres to nanowires
Licensed Content Author	Antoine Lonjon,Philippe Demont,Eric Dantras,Colette Lacabanne
Licensed Content Date	Dec 1, 2012
Licensed Content Volume	358
Licensed Content Issue	23
Licensed Content Pages	5
Start Page	3074
End Page	3078

Type of Use	reuse in a thesis/dissertation
Portion	figures/tables/illustrations
Number of figures/tables/illustrations	1
Format	both print and electronic
Are you the author of this Elsevier article?	No
Will you be translating?	No
Title	Silver Nanowire-enhanced Microflake Electrically Conductive Adhesives for Flexible Hybrid Electronics
Institution name	University of Waterloo
Expected presentation date	Oct 2021
Portions	Fig. 4
Requestor Location	Mr. Hubert Argasinski 5182 Palomar Cres. Mississauga, ON L5R2W9 Canada Attn: Hubert Argasinski
Publisher Tax ID	GB 494 6272 12
Total	0.00 CAD
Terms and Conditions	

INTRODUCTION

1. The publisher for this copyrighted material is Elsevier. By clicking "accept" in connection with completing this licensing transaction, you agree that the following terms and conditions apply to this transaction (along with the Billing and Payment terms and conditions established by Copyright Clearance Center, Inc. ("CCC"), at the time that you opened your Rightslink account and that are available at any time at http://myaccount.copyright.com).

GENERAL TERMS

2. Elsevier hereby grants you permission to reproduce the aforementioned material subject to the terms and conditions indicated.

3. Acknowledgement: If any part of the material to be used (for example, figures) has appeared in our publication with credit or acknowledgement to another source, permission must also be sought from that source. If such permission is not obtained then that material may not be included in your publication/copies. Suitable acknowledgement to the source must be made, either as a footnote or in a reference list at the end of your publication, as follows:

"Reprinted from Publication title, Vol /edition number, Author(s), Title of article / title of chapter, Pages No., Copyright (Year), with permission from Elsevier [OR APPLICABLE SOCIETY COPYRIGHT OWNER]." Also Lancet special credit - "Reprinted from The Lancet, Vol. number, Author(s), Title of article, Pages No., Copyright (Year), with permission from Elsevier."

4. Reproduction of this material is confined to the purpose and/or media for which permission is hereby given.

5. Altering/Modifying Material: Not Permitted. However figures and illustrations may be altered/adapted minimally to serve your work. Any other abbreviations, additions, deletions and/or any other alterations shall be made only with prior written authorization of Elsevier Ltd. (Please contact Elsevier's permissions helpdesk here). No modifications can be made to any Lancet figures/tables and they must be reproduced in full.

6. If the permission fee for the requested use of our material is waived in this instance, please be advised that your future requests for Elsevier materials may attract a fee.

7. Reservation of Rights: Publisher reserves all rights not specifically granted in the combination of (i) the license details provided by you and accepted in the course of this licensing transaction, (ii) these terms and conditions and (iii) CCC's Billing and Payment terms and conditions.

8. License Contingent Upon Payment: While you may exercise the rights licensed immediately upon issuance of the license at the end of the licensing process for the transaction, provided that you have disclosed complete and accurate details of your proposed use, no license is finally effective unless and until full payment is received from you (either by publisher or by CCC) as provided in CCC's Billing and Payment terms and conditions. If full payment is not received on a timely basis, then any license preliminarily granted shall be deemed automatically revoked and shall be void as if never granted. Further, in the event that you breach any of these terms and conditions or any of CCC's Billing and Payment terms and conditions, the license is automatically revoked and shall be void as if never granted. Use of materials as described in a revoked license, as well as any use of the materials beyond the scope of an unrevoked license, may constitute copyright infringement and publisher reserves the right to take any and all action to protect its copyright in the materials.

ELSEVIER LICENSE
TERMS AND CONDITIONS

Sep 20, 2021

This Agreement between Mr. Hubert Argasinski ("You") and Elsevier ("Elsevier") consists of your license details and the terms and conditions provided by Elsevier and Copyright Clearance Center.

License Number	5153240073623
License date	Sep 20, 2021
Licensed Content Publisher	Elsevier
Licensed Content Publication	Materials Science and Engineering: B
Licensed Content Title	Silver nanowires: Synthesis technologies, growth mechanism and multifunctional applications
Licensed Content Author	Pei Zhang,Ian Wyman,Jiwen Hu,Shudong Lin,Zhiwei Zhong,Yuanyuan Tu,Zhengzhu Huang,Yanlong Wei
Licensed Content Date	Sep 1, 2017
Licensed Content Volume	223
Licensed Content Issue	n/a
Licensed Content Pages	23
Start Page	1
End Page	23

Type of Use	reuse in a thesis/dissertation
Portion	figures/tables/illustrations
Number of figures/tables/illustrations	1
Format	both print and electronic
Are you the author of this Elsevier article?	No
Will you be translating?	No
Title	Silver Nanowire-enhanced Microflake Electrically Conductive Adhesives for Flexible Hybrid Electronics
Institution name	University of Waterloo
Expected presentation date	Oct 2021
Portions	Fig. 13
Requestor Location	Mr. Hubert Argasinski 5182 Palomar Cres. Mississauga, ON L5R2W9 Canada Attn: Hubert Argasinski
Publisher Tax ID	GB 494 6272 12
Total	0.00 CAD
Terms and Conditions	

INTRODUCTION

1. The publisher for this copyrighted material is Elsevier. By clicking "accept" in connection with completing this licensing transaction, you agree that the following terms and conditions apply to this transaction (along with the Billing and Payment terms and conditions established by Copyright Clearance Center, Inc. ("CCC"), at the time that you opened your Rightslink account and that are available at any time at http://myaccount.copyright.com).

GENERAL TERMS

2. Elsevier hereby grants you permission to reproduce the aforementioned material subject to the terms and conditions indicated.

3. Acknowledgement: If any part of the material to be used (for example, figures) has appeared in our publication with credit or acknowledgement to another source, permission must also be sought from that source. If such permission is not obtained then that material may not be included in your publication/copies. Suitable acknowledgement to the source must be made, either as a footnote or in a reference list at the end of your publication, as follows:

"Reprinted from Publication title, Vol /edition number, Author(s), Title of article / title of chapter, Pages No., Copyright (Year), with permission from Elsevier [OR APPLICABLE SOCIETY COPYRIGHT OWNER]." Also Lancet special credit - "Reprinted from The Lancet, Vol. number, Author(s), Title of article, Pages No., Copyright (Year), with permission from Elsevier."

4. Reproduction of this material is confined to the purpose and/or media for which permission is hereby given.

5. Altering/Modifying Material: Not Permitted. However figures and illustrations may be altered/adapted minimally to serve your work. Any other abbreviations, additions, deletions and/or any other alterations shall be made only with prior written authorization of Elsevier Ltd. (Please contact Elsevier's permissions helpdesk here). No modifications can be made to any Lancet figures/tables and they must be reproduced in full.

6. If the permission fee for the requested use of our material is waived in this instance, please be advised that your future requests for Elsevier materials may attract a fee.

7. Reservation of Rights: Publisher reserves all rights not specifically granted in the combination of (i) the license details provided by you and accepted in the course of this licensing transaction, (ii) these terms and conditions and (iii) CCC's Billing and Payment terms and conditions.

8. License Contingent Upon Payment: While you may exercise the rights licensed immediately upon issuance of the license at the end of the licensing process for the transaction, provided that you have disclosed complete and accurate details of your proposed use, no license is finally effective unless and until full payment is received from you (either by publisher or by CCC) as provided in CCC's Billing and Payment terms and conditions. If full payment is not received on a timely basis, then any license preliminarily granted shall be deemed automatically revoked and shall be void as if never granted. Further, in the event that you breach any of these terms and conditions or any of CCC's Billing and Payment terms and conditions, the license is automatically revoked and shall be void as if never granted. Use of materials as described in a revoked license, as well as any use of the materials beyond the scope of an unrevoked license, may constitute copyright infringement and publisher reserves the right to take any and all action to protect its copyright in the materials.

ELSEVIER LICENSE
TERMS AND CONDITIONS

Sep 20, 2021

This Agreement between Mr. Hubert Argasinski ("You") and Elsevier ("Elsevier") consists of your license details and the terms and conditions provided by Elsevier and Copyright Clearance Center.

License Number	5153231238326
License date	Sep 20, 2021
Licensed Content Publisher	Elsevier
Licensed Content Publication	Journal of Alloys and Compounds
Licensed Content Title	The mixture of silver nanowires and nanosilver-coated copper micronflakes for electrically conductive adhesives to achieve high electrical conductivity with low percolation threshold
Licensed Content Author	Qian Wang,Shuye Zhang,Guiming Liu,Tiesong Lin,Peng He
Licensed Content Date	Apr 15, 2020
Licensed Content Volume	820
Licensed Content Issue	n/a
Licensed Content Pages	1
Start Page	153184
End Page	0

Type of Use	reuse in a thesis/dissertation
Portion	figures/tables/illustrations
Number of figures/tables/illustrations	1
Format	both print and electronic
Are you the author of this Elsevier article?	No
Will you be translating?	No
Title	Silver Nanowire-enhanced Microflake Electrically Conductive Adhesives for Flexible Hybrid Electronics
Institution name	University of Waterloo
Expected presentation date	Oct 2021
Portions	Fig. 17(a)
Requestor Location	Mr. Hubert Argasinski 5182 Palomar Cres. Mississauga, ON L5R2W9 Canada Attn: Hubert Argasinski
Publisher Tax ID	GB 494 6272 12
Total	0.00 CAD
Terms and Conditions	

INTRODUCTION

1. The publisher for this copyrighted material is Elsevier. By clicking "accept" in connection with completing this licensing transaction, you agree that the following terms and conditions apply to this transaction (along with the Billing and Payment terms and conditions established by Copyright Clearance Center, Inc. ("CCC"), at the time that you opened your Rightslink account and that are available at any time at http://myaccount.copyright.com).

GENERAL TERMS

2. Elsevier hereby grants you permission to reproduce the aforementioned material subject to the terms and conditions indicated.

3. Acknowledgement: If any part of the material to be used (for example, figures) has appeared in our publication with credit or acknowledgement to another source, permission must also be sought from that source. If such permission is not obtained then that material may not be included in your publication/copies. Suitable acknowledgement to the source must be made, either as a footnote or in a reference list at the end of your publication, as follows:

"Reprinted from Publication title, Vol /edition number, Author(s), Title of article / title of chapter, Pages No., Copyright (Year), with permission from Elsevier [OR APPLICABLE SOCIETY COPYRIGHT OWNER]." Also Lancet special credit - "Reprinted from The Lancet, Vol. number, Author(s), Title of article, Pages No., Copyright (Year), with permission from Elsevier."

4. Reproduction of this material is confined to the purpose and/or media for which permission is hereby given.

5. Altering/Modifying Material: Not Permitted. However figures and illustrations may be altered/adapted minimally to serve your work. Any other abbreviations, additions, deletions and/or any other alterations shall be made only with prior written authorization of Elsevier Ltd. (Please contact Elsevier's permissions helpdesk here). No modifications can be made to any Lancet figures/tables and they must be reproduced in full.

6. If the permission fee for the requested use of our material is waived in this instance, please be advised that your future requests for Elsevier materials may attract a fee.

7. Reservation of Rights: Publisher reserves all rights not specifically granted in the combination of (i) the license details provided by you and accepted in the course of this licensing transaction, (ii) these terms and conditions and (iii) CCC's Billing and Payment terms and conditions.

8. License Contingent Upon Payment: While you may exercise the rights licensed immediately upon issuance of the license at the end of the licensing process for the transaction, provided that you have disclosed complete and accurate details of your proposed use, no license is finally effective unless and until full payment is received from you (either by publisher or by CCC) as provided in CCC's Billing and Payment terms and conditions. If full payment is not received on a timely basis, then any license preliminarily granted shall be deemed automatically revoked and shall be void as if never granted. Further, in the event that you breach any of these terms and conditions or any of CCC's Billing and Payment terms and conditions, the license is automatically revoked and shall be void as if never granted. Use of materials as described in a revoked license, as well as any use of the materials beyond the scope of an unrevoked license, may constitute copyright infringement and publisher reserves the right to take any and all action to protect its copyright in the materials.

Bibliography

[1] Stratistics Market Research Consulting Pvt Ltd, “Flexible Electronics - Global Market Outlook (2017-2026),” Dec. 2018.

[2] Grand View Research, “Smart Textile Market Size Worth $5.55 Billion By 2025 | CAGR: 30.4%,” Mar. 2019.

[3] Y. Khan, A. Thielens, S. Muin, J. Ting, C. Baumbauer, and A. C. Arias, “A New Frontier of Printed Electronics: Flexible Hybrid Electronics,” *Advanced Materials*, vol. 32, no. 15. Wiley-VCH Verlag, p. 1905279, 01-Apr-2020.

[4] Y. Li, “MATERIALS SCIENCE: Electronics Without Lead,” *Science (80-.).*, vol. 308, no. 5727, pp. 1419–1420, Jun. 2005.

[5] G. Shi *et al.*, “Highly Sensitive, Wearable, Durable Strain Sensors and Stretchable Conductors Using Graphene/Silicon Rubber Composites,” *Adv. Funct. Mater.*, vol. 26, no. 42, pp. 7614–7625, Nov. 2016.

[6] Q. Liu *et al.*, “High-Quality Graphene Ribbons Prepared from Graphene Oxide Hydrogels and Their Application for Strain Sensors,” *ACS Nano*, vol. 9, no. 12, pp. 12320–12326, Oct. 2015.

[7] S. Lee *et al.*, “Ag nanowire reinforced highly stretchable conductive fibers for wearable electronics,” *Adv. Funct. Mater.*, vol. 25, no. 21, pp. 3114–3121, Jun. 2015.

[8] F. C. Liang *et al.*, “An intrinsically stretchable and ultrasensitive nanofiber-based resistive pressure sensor for wearable electronics,” *J. Mater. Chem. C*, vol. 8, no. 16, pp. 5361–5369, Apr. 2020.

[9] W. Kim *et al.*, “Soft fabric-based flexible organic light-emitting diodes,” *Org. Electron.*, vol. 14, no. 11, pp. 3007–3013, Nov. 2013.

[10] S. Choi *et al.*, “Highly Flexible and Efficient Fabric-Based Organic Light-Emitting Devices for Clothing-Shaped Wearable Displays,” *Sci. Rep.*, vol. 7, no. 1, pp. 1–8, Dec. 2017.

[11] K. Cherenack, C. Zysset, T. Kinkeldei, N. Münzenrieder, and G. Tröster, “Woven Electronic Fibers with Sensing and Display Functions for Smart Textiles,” *Adv. Mater.*, vol. 22, no. 45, pp. 5178–5182, Dec. 2010.

[12] M. Lee *et al.*, “A hybrid piezoelectric structure for wearable nanogenerators,” *Adv. Mater.*, vol. 24, no. 13, pp. 1759–1764, Apr. 2012.

[13] W. Seung *et al.*, “Nanopatterned textile-based wearable triboelectric nanogenerator,” *ACS Nano*, vol. 9, no. 4, pp. 3501–3509, Apr. 2015.

[14] Q. Jiang *et al.*, “MXene electrochemical microsupercapacitor integrated with triboelectric nanogenerator as a wearable self-charging power unit,” *Nano Energy*, vol. 45, pp. 266–272, Mar. 2018.

[15] S. H. Cho, J. Lee, M. J. Lee, H. J. Kim, S. M. Lee, and K. C. Choi, “Plasmonically Engineered Textile Polymer Solar Cells for High-Performance, Wearable Photovoltaics,” *ACS Appl. Mater. Interfaces*, vol. 11, no. 23, pp. 20864–20872, Jun. 2019.

[16] N. Zhang *et al.*, “A Wearable All-Solid Photovoltaic Textile,” *Adv. Mater.*, vol. 28, no. 2, pp. 263–269, Jan. 2016.

[17] Z. Yang, J. Deng, X. Sun, H. Li, and H. Peng, “Stretchable, wearable dye-sensitized solar cells,” *Adv. Mater.*, vol. 26, no. 17, pp. 2643–2647, May 2014.

[18] S. Ajami and L. Khaleghi, “A review on equipped hospital beds with wireless sensor networks for reducing bedsores,” *J. Res. Med. Sci.*, vol. 20, no. 10, pp. 1007–1015, Oct. 2015.

[19] T. Linz, C. Kallmayer, R. Aschenbrenner, and H. Reichl, “Embroidering electrical interconnects with conductive yarn for the integration of flexible electronic modules into fabric,” in *Proceedings - International Symposium on Wearable Computers, ISWC*, 2005, vol. 2005, pp. 86–89.

[20] E. P. Simon, C. Kallmayer, M. Schneider-Ramelow, and K. D. Lang, “Development of a multi-terminal crimp package for smart textile integration,” in *2012 4th Electronic System-Integration Technology Conference, ESTC 2012*, 2012.

[21] J. Leśnikowski, “Research on poppers used as electrical connectors in high speed textile transmission lines,” *Autex Res. J.*, vol. 16, no. 4, pp. 228–235, Dec. 2016.

[22] I. Trindade *et al.*, “Design and Evaluation of Novel Textile Wearable Systems for the Surveillance of Vital Signals,” *Sensors*, vol. 16, no. 10, p. 1573, Sep. 2016.

[23] R. Aradhana, S. Mohanty, and S. K. Nayak, “A review on epoxy-based electrically conductive adhesives,” *Int. J. Adhes. Adhes.*, vol. 99, p. 102596, Jun. 2020.

[24] Q. Yan, M. Zhou, and H. Fu, “A reversible and highly conductive adhesive: Towards self-healing and recyclable flexible electronics,” *J. Mater. Chem. C*, vol. 8, no. 23, pp. 7772–7785,

Jun. 2020.

[25] R. Ma *et al.*, “Carbon-Nanotube/Silver Networks in Nitrile Butadiene Rubber for Highly Conductive Flexible Adhesives,” *Adv. Mater.*, vol. 24, no. 25, pp. 3344–3349, Jul. 2012.

[26] J. Li, J. K. Lumpp, R. Andrews, and D. Jacques, “Aspect ratio and loading effects of multiwall carbon nanotubes in epoxy for electrically conductive adhesives,” *J. Adhes. Sci. Technol.*, vol. 22, no. 14, pp. 1659–1671, Sep. 2008.

[27] H. P. Wu *et al.*, “High conductivity of isotropic conductive adhesives filled with silver nanowires,” *Int. J. Adhes. Adhes.*, vol. 26, no. 8, pp. 617–621, Dec. 2006.

[28] R. Durairaj and L. W. Man, “Effect of epoxy and filler concentrations on curing behaviour of isotropic conductive adhesives,” *J. Therm. Anal. Calorim.*, vol. 105, no. 1, pp. 151–155, Jul. 2011.

[29] M. Hongru, Y. Shaocun, L. Zhe, T. Xun, M. Lei, and M. Yanqing, “Polyurethane-based flexible conductive adhesives,” in *2017 18th International Conference on Electronic Packaging Technology (ICEPT)*, 2017, pp. 448–450.

[30] G. Beaucarne *et al.*, “Innovative Cell Interconnection Based on Ribbon Bonding of Busbar-less Cells Using Silicone-based Electrically Conductive Adhesives,” in *Energy Procedia*, 2015, vol. 67, pp. 185–193.

[31] G. Beaucarne *et al.*, “Study of compatibility of silicone-based electrically conductive adhesives and conductive backsheets for MWT modules,” in *Energy Procedia*, 2014, vol. 55, pp. 444–450.

[32] Y. Li and C. P. Wong, “Recent advances of conductive adhesives as a lead-free alternative in electronic packaging: Materials, processing, reliability and applications,” *Materials Science and Engineering R: Reports*, vol. 51, no. 1–3. Elsevier BV, pp. 1–35, 30-Jan-2006.

[33] Y. H. Wang, N. N. Xiong, H. Xie, Y. Z. Zhao, and J. Li, “New insights into silver nanowires filled electrically conductive adhesives,” *Journal of Materials Science: Materials in Electronics*, vol. 26, no. 2. Springer New York LLC, pp. 621–629, 09-Nov-2014.

[34] D. Lu and C. P. Wong, “Electrically conductive adhesives (ECAs),” in *Materials for Advanced Packaging, Second Edition*, Springer International Publishing, 2016, pp. 421–468.

[35] Y. H. Wang *et al.*, “A comprehensive study of silver nanowires filled electrically conductive

adhesives," *J. Mater. Sci. Mater. Electron.*, vol. 26, no. 10, pp. 7927–7935, Jul. 2015.

[36] B. Meschi Amoli *et al.*, "SDS-stabilized graphene nanosheets for highly electrically conductive adhesives," *Carbon N. Y.*, vol. 91, pp. 188–199, May 2015.

[37] J. Trinidad, L. Chen, A. Lian, and B. Zhao, "Solvent presence and its impact on the lap-shear strength of SDS-decorated graphene hybrid electrically conductive adhesives," *Int. J. Adhes. Adhes.*, vol. 78, pp. 102–110, Oct. 2017.

[38] A. L. Bernassau, D. Hutson, C. E. M. Démoré, and S. Cochran, "Characterization of an epoxy filler for piezocomposites compatible with microfabrication processes," *IEEE Trans. Ultrason. Ferroelectr. Freq. Control*, vol. 58, no. 12, pp. 2743–2748, Dec. 2011.

[39] L. Rivière, A. Lonjon, E. Dantras, C. Lacabanne, P. Olivier, and N. R. Gleizes, "Silver fillers aspect ratio influence on electrical and thermal conductivity in PEEK/Ag nanocomposites," *Eur. Polym. J.*, vol. 85, pp. 115–125, Dec. 2016.

[40] A. Lonjon, P. Demont, E. Dantras, and C. Lacabanne, "Low filled conductive P(VDF-TrFE) composites: Influence of silver particles aspect ratio on percolation threshold from spheres to nanowires," *J. Non. Cryst. Solids*, vol. 358, no. 23, pp. 3074–3078, Dec. 2012.

[41] B. Meschi Amoli, A. Hu, N. Y. Zhou, and B. Zhao, "Recent progresses on hybrid micro–nano filler systems for electrically conductive adhesives (ECAs) applications," *J. Mater. Sci. Mater. Electron.*, vol. 26, no. 7, pp. 4730–4745, Jul. 2015.

[42] L. Li and J. E. Morris, "Electrical conduction models for isotropically conductive adhesive joints," *IEEE Trans. Components Packag. Manuf. Technol. Part A*, vol. 20, no. 1, pp. 3–8, Mar. 1997.

[43] H. Jiang, K. S. Moon, Y. Li, and C. P. Wong, "Surface functionalized silver nanoparticles for ultrahigh conductive polymer composites," *Chem. Mater.*, vol. 18, no. 13, pp. 2969–2973, Jun. 2006.

[44] C. Li, E. T. Thostenson, and T. W. Chou, "Dominant role of tunneling resistance in the electrical conductivity of carbon nanotube-based composites," *Appl. Phys. Lett.*, vol. 91, no. 22, p. 223114, Nov. 2007.

[45] H. W. Cui, Q. Fan, and D. S. Li, "Surface functionalization of micro silver flakes and their application in electrically conductive adhesives for electronic package," *Int. J. Adhes. Adhes.*,

vol. 48, pp. 177–182, Jan. 2014.

[46] S. Zhang, X. Xu, T. Lin, and P. He, “Recent advances in nano-materials for packaging of electronic devices,” *J. Mater. Sci. Mater. Electron.*, vol. 30, no. 15, pp. 13855–13868, Aug. 2019.

[47] J. K. W. Sandler, J. E. Kirk, I. A. Kinloch, M. S. P. Shaffer, and A. H. Windle, “Ultra-low electrical percolation threshold in carbon-nanotube-epoxy composites,” *Polymer (Guildf).*, vol. 44, no. 19, pp. 5893–5899, Aug. 2003.

[48] A. Nogales *et al.*, “Low Percolation Threshold in Nanocomposites Based on Oxidized Single Wall Carbon Nanotubes and Poly(butylene terephthalate),” *Macromolecules*, vol. 37, no. 20, pp. 7669–7672, Oct. 2004.

[49] B. M. Amoli, E. Marzbanrad, A. Hu, Y. N. Zhou, and B. Zhao, “Electrical Conductive Adhesives Enhanced with High-Aspect-Ratio Silver Nanobelts,” *Macromol. Mater. Eng.*, vol. 299, no. 6, pp. 739–747, Jun. 2014.

[50] C. Yang, C. P. Wong, and M. M. F. Yuen, “Printed electrically conductive composites: Conductive filler designs and surface engineering,” *J. Mater. Chem. C*, vol. 1, no. 26, pp. 4052–4069, Jul. 2013.

[51] A. Lonjon, P. Demont, E. Dantras, and C. Lacabanne, “Low filled conductive P(VDF-TrFE) composites: Influence of silver particles aspect ratio on percolation threshold from spheres to nanowires,” *J. Non. Cryst. Solids*, vol. 358, no. 23, pp. 3074–3078, Dec. 2012.

[52] L. Ye, Z. Lai, J. Liu, and A. Thölén, “Effect of Ag particle size on electrical conductivity of isotropically conductive adhesives,” *IEEE Trans. Electron. Packag. Manuf.*, vol. 22, no. 4, p. 251, 1999.

[53] H.-M. Ren *et al.*, “One-Step Preparation of Silver Hexagonal Microsheets as Electrically Conductive Adhesive Fillers for Printed Electronics,” *ACS Appl. Mater. Interfaces*, vol. 7, no. 24, pp. 13685–13692, Jun. 2015.

[54] C. Yang *et al.*, “Fractal dendrite-based electrically conductive composites for laser-scribed flexible circuits,” *Nat. Commun.*, vol. 6, no. 1, p. 8150, Nov. 2015.

[55] Y. Sun, B. Gates, B. Mayers, and Y. Xia, “Crystalline Silver Nanowires by Soft Solution Processing,” *Nano Lett.*, vol. 2, no. 2, pp. 165–168, Feb. 2002.

[56] J. Lu, D. Liu, and J. Dai, “Preparation of highly conductive silver nanowires for electrically conductive adhesives,” *J. Mater. Sci. Mater. Electron.*, vol. 30, no. 16, pp. 15786–15794, Aug. 2019.

[57] P. Zhang *et al.*, “Silver nanowires: Synthesis technologies, growth mechanism and multifunctional applications,” *Materials Science and Engineering B: Solid-State Materials for Advanced Technology*, vol. 223. Elsevier Ltd, pp. 1–23, 01-Sep-2017.

[58] Y. Sun, B. Mayers, T. Herricks, and Y. Xia, “Polyol synthesis of uniform silver nanowires: A plausible growth mechanism and the supporting evidence,” *Nano Lett.*, vol. 3, no. 7, pp. 955–960, Jul. 2003.

[59] Y. Sun and Y. Xia, “Large-Scale Synthesis of Uniform Silver Nanowires Through a Soft, Self-Seeding, Polyol Process,” *Adv. Mater.*, vol. 14, no. 11, pp. 833–837, Jun. 2002.

[60] X. S. Li, X. Z. Xiang, L. Wang, and X. J. Bai, “Conductivity and mechanical properties of conductive adhesive with silver nanowires,” *Rare Met.*, vol. 37, no. 3, pp. 191–195, Mar. 2018.

[61] P. Lee *et al.*, “Highly stretchable and highly conductive metal electrode by very long metal nanowire percolation network,” *Adv. Mater.*, vol. 24, no. 25, pp. 3326–3332, Jul. 2012.

[62] X.-Y. Zeng, Q.-K. Zhang, R.-M. Yu, and C.-Z. Lu, “A New Transparent Conductor: Silver Nanowire Film Buried at the Surface of a Transparent Polymer,” *Adv. Mater.*, vol. 22, no. 40, pp. 4484–4488, Oct. 2010.

[63] T. Kim, Y. W. Kim, H. S. Lee, H. Kim, W. S. Yang, and K. S. Suh, “Uniformly interconnected silver-nanowire networks for transparent film heaters,” *Adv. Funct. Mater.*, vol. 23, no. 10, pp. 1250–1255, Mar. 2013.

[64] Q. Wang, S. Zhang, G. Liu, T. Lin, and P. He, “The mixture of silver nanowires and nanosilver-coated copper micronflakes for electrically conductive adhesives to achieve high electrical conductivity with low percolation threshold,” *J. Alloys Compd.*, vol. 820, p. 153184, Apr. 2020.

[65] H. Ma *et al.*, “Silver Flakes and Silver Dendrites for Hybrid Electrically Conductive Adhesives with Enhanced Conductivity,” *J. Electron. Mater.*, vol. 47, no. 5, pp. 2929–2939, May 2018.

[66] A. A. Mohammed, “Development of a new Stretchable and Screen Printable Conductive Ink,” University of Maryland, College Park, 2017.

[67] D. Chen, X. Qiao, X. Qiu, F. Tan, J. Chen, and R. Jiang, “Effect of silver nanostructures on the resistivity of electrically conductive adhesives composed of silver flakes,” *J. Mater. Sci. Mater. Electron.*, vol. 21, no. 5, pp. 486–490, May 2010.

[68] R. Aradhana, S. Mohanty, and S. K. Nayak, “High performance epoxy nanocomposite adhesive: Effect of nanofillers on adhesive strength, curing and degradation kinetics,” *Int. J. Adhes. Adhes.*, vol. 84, pp. 238–249, Aug. 2018.

[69] C. Chen, L. Wang, R. Li, G. Jiang, H. Yu, and T. Chen, “Effect of silver nanowires on electrical conductance of system composed of silver particles,” *J. Mater. Sci.*, vol. 42, no. 9, pp. 3172–3176, May 2007.

[70] Z. X. Zhang, X. Y. Chen, and F. Xiao, “The sintering behavior of electrically conductive adhesives filled with surface modified silver nanowires,” *J. Adhes. Sci. Technol.*, vol. 25, no. 13, pp. 1465–1480, 2011.

[71] H. Xie, N. Xiong, Y. Zhao, and Y. Wang, “Effect of silver nanowires on the resistivity of electronically conductive adhesives,” *Xiyou Jinshu Cailiao Yu Gongcheng/Rare Met. Mater. Eng.*, vol. 45, no. 10, pp. 2503–2508, Oct. 2016.

[72] Q. Chen *et al.*, “Ultrasonic bending of silver nanowires,” *ACS Nano*, vol. 14, no. 11, pp. 15286–15292, Nov. 2020.

[73] H.-W. Chiang, C.-L. Chung, L.-C. Chen, Y. Li, C. P. Wong, and S.-L. Fu, “Processing and shape effects on silver paste electrically conductive adhesives (ECAs),” *http://dx.doi.org/10.1163/1568561054352487*, vol. 19, no. 7, pp. 565–578, 2012.

[74] B. Meschi Amoli, J. Trinidad, A. Hu, Y. N. Zhou, and B. Zhao, “Highly electrically conductive adhesives using silver nanoparticle (Ag NP)-decorated graphene: the effect of NPs sintering on the electrical conductivity improvement,” *J. Mater. Sci. Mater. Electron.*, vol. 26, no. 1, pp. 590–600, Jan. 2015.

[75] A. Redmann, V. Damodaran, F. Tischer, P. Prabhakar, and T. A. Osswald, “Evaluation of Single-Lap and Block Shear Test Methods in Adhesively Bonded Composite Joints,” *J. Compos. Sci. 2021, Vol. 5, Page 27*, vol. 5, no. 1, p. 27, Jan. 2021.

[76] J. Atkinson and I. A. Goldthorpe, “Near-infrared properties of silver nanowire networks,” *Nanotechnology*, vol. 31, no. 36, p. 7, Sep. 2020.

[77] J. J. Chen *et al.*, “Structural regulation of silver nanowires and their application in flexible electronic thin films,” *Mater. Des.*, vol. 154, pp. 266–274, Sep. 2018.

[78] G. Deignan and I. A. Goldthorpe, “The dependence of silver nanowire stability on network composition and processing parameters,” *RSC Adv.*, vol. 7, no. 57, pp. 35590–35597, Jul. 2017.

[79] M. Inoue, H. Muta, S. Yamanaka, and K. Suganuma, “Temperature dependence of electrical resistivity of isotropic conductive adhesive composed of an epoxy-based binder,” in *Proceedings of International Symposium on High Density Packaging and Microsystem Integration 2007, HDP’07*, 2007.

[80] M. Muaz, B. Nasaruddin, S. H. Sheikh, M. Fadzullah, G. Omar, and Z. Mustafa, “The effect of aspect ratio on multi-walled carbon nanotubes filled epoxy composite as electrically conductive adhesive,” 2019.

[81] M. A. Yokus, R. Foote, and J. S. Jur, “Printed Stretchable Interconnects for Smart Garments: Design, Fabrication, and Characterization,” *IEEE Sens. J.*, vol. 16, no. 22, pp. 7967–7976, Nov. 2016.

[82] A. Mohammed and M. Pecht, “A stretchable and screen-printable conductive ink for stretchable electronics,” *Appl. Phys. Lett.*, vol. 109, no. 18, p. 184101, Nov. 2016.

[83] B. J. Perelaer, A. W. M. de Laat, C. E. Hendriks, and U. S. Schubert, “Inkjet-printed silver tracks: low temperature curing and thermal stability investigation,” *J. Mater. Chem.*, vol. 18, no. 27, pp. 3209–3215, Jul. 2008.